uOttawa

L'Université canadienne
Canada's university

FACULTÉ DES ÉTUDES SUPÉRIEURES ET POSTOCTORALES

u Ottawa

L'Université canadienne
Canada's university

FACULTY OF GRADUATE AND POSDOCTORAL STUDIES

Vijaya Lakshmi Guruswamy
AUTEUR DE LA THÈSE / AUTHOR OF THESIS

M.C.S.
GRADE / DEGREE

School of Information Technology and Engineering
FACULTÉ, ÉCOLE, DÉPARTEMENT / FACULTY, SCHOOL, DEPARTMENT

Measurement and Modelling of Haptic Textures
TITRE DE LA THÈSE / TITLE OF THESIS

Wonsook Lee
DIRECTEUR (DIRECTRICE) DE LA THÈSE / THESIS SUPERVISOR

Jochen Lang
CO-DIRECTEUR (CO-DIRECTRICE) DE LA THÈSE / THESIS CO-SUPERVISOR

Peter X. Liu

Shervin Shirmohammadi

Gary W. Slater
Le Doyen de la Faculté des études supérieures et postdoctorales / Dean of the Faculty of Graduate and Postdoctoral Studies

Measurement and Modelling of Haptic Textures

By

Vijaya Lakshmi Guruswamy

A thesis submitted to

Faculty of Graduate Studies and Postdoctoral Studies

In partial fulfilment of the requirements for the degree

Masters in Computer Science

Ottawa-Carleton Institute for Computer Science

School of Information Technology and Engineering

University of Ottawa

Ottawa, Ontario, Canada

December 04, 2009.

Your file Votre référence
ISBN: 978-0-494-61162-3
Our file Notre référence
ISBN: 978-0-494-61162-3

Abstract

Haptic texture allows the user to feel the fine surface details of an object. In the absence of haptic texture, irrespective of the appearance of a virtual object, the object feels smooth. Haptic texture conveys these surface details of an object in terms of material variables - roughness and compliance. Roughness can be inferred from irregularities in the surface structure, whereas compliance can be determined from the deformation of the object when a force is applied. To model realistic haptic textures, one needs to incorporate these material variables from real world samples. Haptic texture modelling, which accurately represents the material variables from real world samples, can be a challenging task. We introduce a vibrotactile model to represent haptic textures and a statistical approach to estimate compliance from real world measurements. We measure the material variables from real life objects by simply stroking the surface with a hand-held probe. We claim that our vibrotactile model is simple and can represent both surfaces with identifiable features and stochastic nature. Our compliance estimation is carried out by analyzing the linear relationship between force and acceleration. The estimated compliance coefficients serve as a good heuristic model to render the stiffness of textures.

Acknowledgements

I would like to thank my supervisor, Dr. WonSook Lee, and co-supervisor, Dr. Jochen Lang, for their guidance and support throughout my research. I would also take the opportunity to acknowledge my sincere thanks to them for providing all the necessary facilities and financial support required for this task. My sincere thank goes to Sheldon Andrews, an alumnus of University of Ottawa, for his scanning system and Jilin Zhou, a PhD. candidate in the Discover Laboratory at the University of Ottawa, for his guidance regarding freedom 6s device. I would like to express my appreciation to Mauricio Vines and other colleagues from Computer Graphics and Applications Lab. Finally I would like to thank my family members and friends for their inspiration and motivation towards the completion of this thesis.

Table of Contents

List of Tables

List of Figures

List of Acronyms

WHaT	Wireless Haptic Texture Sensor
IIR	Infinite-Impulse-Response
FIR	Finite Impulse Response
ARMA	Autoregressive Moving Average Models
PLD	Programmable Logic Device
DOF	Degrees of Freedom
2D	Two Dimensional
3D	Three Dimensional

Chapter 1: Introduction

1.1 Scope and Overview

Different properties of a material can be explored through different sense. Some of the properties such as size, shape, color etc., can be examined through vision, whereas, other properties like texture, compliance etc., are investigated through the sense of touch. Haptic refers to "the sense of touch" according to the Oxford dictionary [Oxfo09]. Haptic perception derives from tactile and kinesthetic sensations. In a physical environment, these sensations arise when a human comes into contact with the environment. Tactile sensations are generated when skin touches an object. On the other hand, kinesthetic sensations are generated in the muscles and joints due to force and motion from interacting with an object.

Touch is unique since it senses and manipulates the physical environment simultaneously. Therefore, if touch is enabled in virtual environment, it gives high interactivity. The sense of touch can be stimulated through haptics by computer manipulated force feedback that triggers both tactile and kinesthetic sensation to the perceiver who manipulates and explores characteristics of an object. These sensations are triggered in the perceiver's fingertips by the haptic interface through computer-controlled mechanical forces [Robl08]. Tactile feedback produce forces on the user's skin

directly, which the user is able to perceive through embedded receptors in the skin called mechanoreceptors. With kinesthetic feedback, the user can feel the force exerted to the muscles in correlation with the movement of the perceiver. Tactile feedback and kinesthetic feedback are together referred to force-feedback in computer haptics terminology [Harr09]. The introduction of the sense of touch in virtual environments through haptic interfaces is enhancing human-computer interaction.

A Haptic interface is defined as a programmable peripheral device that is capable of generating synthetic stimulation of the sense of touch through force-feedback. Most of the haptic interfaces employ special tools that help a user to interact with ease. Robles-De-La-Torre referred to these tools as *manipulandums:* "to experience the haptic variables, a perceiver wears or handles the manipulandums" [Robl08]. Most haptic interfaces are of 1 Degrees-of-freedom (DOF), 2 DOF, 3 DOF and 6 DOF depending on their ability of manipulandums' workspace. The DOF may refer to either the ability of the haptic interfaces to keep track of user's position and orientation, or to output forces to the user in three dimensional space. Commonly used haptic interfaces are 3 DOF, with 3DOF force output and 6DOF positional sensing, with a pen like interface, for example, PHANTOM Omni, a desktop which provides flexibility to the user in interacting with the application.

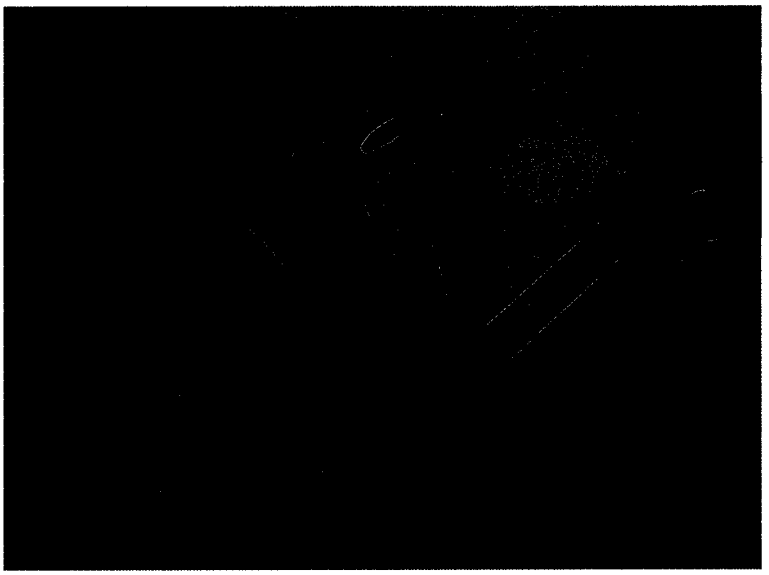

Figure 1: PHANTOM® Omni haptic interface from SensAble Technologies

Haptic Interfaces have a wide range of applications in various fields such as teleoperation or telerobotics, medical training simulations, video gaming applications and e-commerce. In telerobotics, haptic devices are used to assist the operator to control a remote object. Haptics technology was pioneered in telerobotics systems. In medical training simulations, haptic interfaces are employed by medical practitioners to train their assistants for complicated surgery. Use of haptic technology in the field of medical science saves costs such as hospital expenses, surgeons training etc. [Okam04]. Haptic technology is highly benefitted to the video game industry as it provides high level interactivity to the end user. For instance, force feedback joysticks have already come into the market. In all of the above, haptic interfaces increase realism of the environment by enhancing details. In the online economy of e-commerce, in particular with the textile industry, haptic interfaces have the potential to provide remote level interaction through tactile display characteristics [Harr09]. Haptics has found way into touchable maps for the blind to feel the city [Harr09].

1.2 Motivation

One of the major roles of haptic interfaces in virtual environment is to convey object and material cues such as texture, shape, size, compliance and weight of the object during haptic exploration with its force-feedback characteristic. A human performs different exploration procedures based on the object attribute of interest in the physical world. For example, the texture of the object is perceived by lateral motion, the compliance or hardness of the object is perceived by deforming the object through pressure, the temperature of the object is estimated by static touch, and the global shape of an object is determined by enclosure [LeKl87a]. Thus with the advent of computer haptics, significant material and object features can potentially be presented in virtual reality applications.

Rendering of haptic phenomena is often done based on how the representations of the physical attributes of objects are modeled in the application environment, including stiffness and roughness. It has been shown that detailed surface characteristics have a significant effect on object identification [KlLe99], and that in the absence of structural feedback, material detail is solely relied on for identification. This indicates that the realism of virtual objects may be increased by assigning realistic properties used in surface interaction, which encourage us to incorporate reality-based modeling. According to Pai et al. [PLLW99] reality-based modeling can be stated as "effective computational models of real, physical objects based on actual measurements". Reality based models are derived from experimental measurements captured from the physical or real environments. Reality based models are known to be effective in simulating the realistic

feel of real environments in haptic perception of the world [CoHo07]. When modelling haptic material cues - texture and compliance, from reality-based models, data from the physical environment may be recorded through various sensors potentially using even the haptic interface itself. Textures may be recorded while stroking the surface. Different modes of contact with the specimen (material under test) have been investigated when measuring the compliance of the surface, for example by actively tapping on the surface of the specimen with a finger [BaHe08], or with the help of a stylus based instrument mounted with an external device to measure the force or torque required to deform the specimen within the elastic limit [OkCD01]. The goal of our research to introduce a reality-based approach for, both, vibrotactile feedback that represents textures of varying nature, and estimation of the compliance. Compliance is defined as the inverse of stiffness. We measure the stiffness of an object by observing dynamic behavior via scanning.

Generating haptic feedback through vibrations to convey the tactile characteristics of an object is one of the widely used and effective techniques in virtual reality applications. Vibration signals contribute a significant role both in real world scenarios and perceptual analysis. For example, we experience vibrations during contact with our physical environment. One source of vibrations is stroking a surface as we sense and explore our environment. In this process, we may, for example use our fingers, finger nails or a tool to excite a vibration response. The vibrations during a stroke convey information about the surface finish and patterns in the surface structure. The study from neuroscience reveals that vibrations play a major role in tactual sensation when an intermediate probe or tool is used to explore. The Human nerve endings are highly responsive for the

perception of vibrations sensing vibration to 1 kHz and down to less than 1 micrometer in amplitude [JoLL82]. Our goal is to model the vibrations in the virtual environment based on what is observed in the real-world scenario with flexible approach and less input data. Vibration feedback is a notion of generating vibration waveforms to the end-user who manipulates the object in the virtual environment through existing haptic interfaces without any additional overhead on the hardware. The integration of vibrotactile feedback with the force feedback adds a new dimension of reality to virtual environments by considerably increasing the perception of "touch" without any additional complexity and cost to the interface. General force feedback consists of generating force proportional to the penetration distance, i.e. a virtual wall modeled as surface stiffness. Vibrotactile feedbacks that are generated to the task related context, such as stroking texture with a stylus, are superimposed on top of the force feedback. Vibration feedback can also be generated with very simple means [HaMA07] and is used in game controllers, cell phones and mobile devices because of its efficacy. However, the role of vibration feedback is not extensively studied towards haptic texture applications.

In general, when one explores the surface texture of the object either through direct contact for example with a bare finger or with the stylus, the surface deforms to a small extent as a result of natural characteristics of the specimen. Integrating the contact stiffness with our vibrotactile texture makes the virtual environment more realistic. To measure this, compliance is used and it is one of the goals of this thesis. Compliance is the inverse of stiffness. The compliance of an object can be measured by the degree of deformation the object undergoes in proportion to the applied force. Thus the effective perceptual discrimination of compliance requires both force and displacement as

parameters [BaHe08]. Interacting with compliant materials – stiffness or compliance has been considered widely in haptic perception. However, a very limited number of studies are directed in the research of compliance comparatively with other properties that are explored by touch.

1.3 Our Approach

Haptic textures can be made to feel more realistic by incorporating data from physical measurements. Modeling haptic cues from captured samples can be a complex task. Our intent is to integrate a vibrotactile model into haptics for all surface textures irrespective of their characteristics and also to introduce compliance by merely stroking the surface with the stylus. Integrating reality based models into a virtual environment enriches the application. We follow an approach of modelling vibrotactile texture through the use of Infinite Impulse Response (IIR) digital filters and estimate compliance by a linear function relating force and acceleration.

1.4 Contribution

This thesis makes two key contributions:

- We propose a novel idea for modeling haptic vibration texture using digital filters which can simulate both stochastic and patterned textures.

  This part of the thesis work has been presented at the IEEE International Workshop on Haptic Audio-Visual Environments and Games (HAVE 2009).

- The tactile scanning system [Andr07] is employed to estimate the compliance as the average slope approximating a linear function relating acceleration to force [LaAn09]. We contributed experiments supporting the above approach.

Both of these contributions employ reality-based modeling.

1.5 Thesis Overview

The remainder of this thesis is organized as follows: Chapter 2 reviews the state of art on tactile sensation and perception in virtual environments. It also provides a brief discussion of haptic texture rendering and vibrotactile feedback models. Chapter 3 presents background information on an existing acquisition system that we used for measuring force-acceleration profiles. Chapter 4 develops our IIR-filter-based haptic vibrotactile texture model. Chapter 5 describes our estimation methods for the contact stiffness of an object. Chapter 6 illustrates results and analysis of our model. We conclude and provide an outlook on future work in Chapter 7.

Chapter 2: Related Work

This chapter provides an overview on perceptional analysis of texture, synthetic generation of texture, various haptic texture rendering techniques and vibration feedback modeling in a virtual environment. Section 2.1 focuses on the research conducted on perception of textures and experimental studies to analyze the perception in terms of description, exploratory methods used in traversing the surface, and distribution and size of surface features. Section 2.2 describes traditional haptic texture rendering methods and the algorithms available to generate texture oriented force. Section 2.3 talks about reality-based modeling in a virtual environment and the importance of vibration feedback in haptic interfaces.

2.1 Tactile Sensing and Perception

According to Chi et al., "Surface texture refers to the local deviations of a surface from its ideal shape" [CBOZ04]. The distinctive character of texture gives the feel of the surface that uniquely identifies the object. Generally an object is conceptualized in the physical world through touch, based on its size, shape, texture and compliance. On the other hand, haptic perception of an object mainly depends on from the mechanical signals such as contact force, torques, stiffness of materials and geometry of objects etc., [Robl08]. A significant number of fundamental experiments were carried on the perception of texture to determine the number of required dimensions, for instance,

rough- smooth, soft- hard, bumpy- coarse, flat-fuzzy, grainy-slick, to efficiently represent the properties of the texture. Hollins et al. [HBKY00] performed studies to determine the dimensionality of tactile surface texture based on the adjective analysis. Twenty subjects were asked to sort seventeen tactile stimuli into three to seven categories based on the perceived dissimilarity on each of five scale adjective rate - smooth, hard, slippery, flat and warm. Subject's data were then fitted into a multidimensional space using regression analysis. The data fit showed that two orthogonal dimensions, roughness - smoothness and hardness – softness, were more dominant with a third weak dimension as sticky - slippery. In their study, the perceiver's fingertip remained static throughout the experiment while the stimulus was moved across the index finger with a constant speed. A similar study of identifying perceptual dimensions for tactile textures but limiting to a very specific type of material, car-seat fabrics, was done by Picard et al [PDVG03]. Their work is based on the interdependence of tactile texture perception based on perceivers hand movement. Participants were allowed to explore the surfaces actively using lateral motion instead of passive stimulation condition by Hollins et al. [HBKY00]. The results showed that the soft-hard dimension contributed as the prominent dimension in texture space followed by the thin-thick (in terms of density) dimension orthogonal to the soft-hard dimension. However, since they limited their study to a very specific kind of material, these dimensions are dependent on the stimulus included in the given set and hence could not be applicable to the textures in general.

More recently, Bergmann Tiest et al [TiKa06] explored a free sorting task of 124 material samples, spanning a broad range of tactile materials, to measure the relevant number of dimensions for haptic perception. Each sample was explored in duplex sets: one set was

used for psychological characterization while the other set was used for the physical measurements of material parameters. For the physical measurement, compressibility and roughness are picked as parameters. For the psychological experiment, twenty subjects were allowed to dynamically touch and explore the surface of the material samples to sort them into groups based on the perceived similarity. The results from the psychological exploration group and from the physical measurements were fitted reasonably into a multidimensional space. They estimated the relevant number of dimensions for haptic perception of materials to be four without specifically relating them to physical parameters but a logarithmic approximation was observed between physical measures with the perceived property.

An extensive study on the perceptual difference of roughness by humans was carried out by Lederman and Klatzky [LeKl98b]. In the experiment the participants were asked to explore a textured surface through a bare finger and a rigid link, interposed between skin and the surface. The authors' idea was based upon Katz's work [Katz89] which stipulated that roughness perception is a combination of spatial and vibratory codes during direct interaction with the skin. When the finger directly comes in contact with the textured surface, a strong correlation between the spatial gradient on the skin and the spatial gradient [HFRY93] on the textured surface exists which results in both spatial and vibratory coding. Lederman and Klatzky [LeKl98b] analyzed that when the surface is explored through a rigid structure this correlation is eliminated resulting only in vibratory coding. Hence, by letting the user explore the textured surface through a probe, roughness perception is limited to vibratory coding. In general, the spatial-intensive coding contributes more to the roughness perception of macro-textures, whereas, vibratory

coding of roughness perception contributes to the micro-level textures whose elements are on the order of microns.

Klatzky and Lederman [KlLe99] conducted experiments on the relative sensitivity of vibrotactile versus spatial intensive coding[1]. They performed a statistical comparison of the subjects' roughness perception versus texture spacing with the aid of a logarithmic graph. While comparing they used magnitude estimation and roughness discrimination method with both bare finger exploration (direct contact) and a rigid probe. They concluded that when explored through a rigid link, roughness starts increasing with the increase in texture spacing until it attains the maximum roughness value and then roughness begins decreasing. It proved that the probe efficiently transmits vibratory information to the skin that reflects perturbations of the textured surface. However, these vibratory cues are in turn altered by a number of other possible factors such as variance in the surface geometry, probe compliance, contact size and contact shape.

Lederman et al [LKHG00] hypothesized that the diameter of the probe and the applied normal force significantly influence the perceived roughness. The roughness (peak) perception is higher for smaller probes and it occurs at smaller texture spacing values. Similarly, roughness perception is higher for larger force values. To conclude, the vibratory coding can effectively represent roughness and is intimately related to both geometry and other dynamic factors [LKHG*03].

---

[1]Klatzky and Lederman defined spatial intensive coding as:" By spatial intensive, we mean processing that begins with a representation of the layout of textural elements in space but culminates in an integrated representation of magnitude"[KlLe99]

Much research has been done on the virtual haptic texture generation and the experience of roughness that results from a variety of synthesis approaches. Synthetic texture generation models in the haptics are based on the techniques used in computer graphics texture generation [FrBa96]. Jansson et al. [JPCK*99] employed an experimental study to analyze the perceptional difference between virtual textures and real textures. Their objective was to find relationship between the physical parameters and perceived property of the stimuli. Using PHANTOM display, they simulated virtual sandpapers from the data collected by exploring real sandpapers of varying grit sizes. The participants for their experimental study fall under twofold: blind and sighted. The results demonstrated that both the real and virtual sandpapers were perceived by all the participants in a similar fashion. The participants employed a similar exploration technique i.e. used a stylus to explore real and virtual sandpapers. However, the virtual sandpapers are perceived to be rougher than their corresponding real-sandpapers.

Minsky and Lederman [MiLe96] studied the roughness perception by using their "Sandpaper System". In their experiment, they investigated the relationship between perceived roughness and physical parameters. In their experiment they varied the size of grating (0.7~10 mm) and the amplitude (0.17N~ 3.74N) of the applied force. Participants were asked to explore virtual textures by using only lateral forces with a 2-DOF joystick. To verify the perceptual differences, a set of thirty square gratings was employed. Their result showed that the perceived magnitude of roughness was mostly dependent upon the amplitude of the lateral force exerted on the subject's hand rather than on the grating feature size. A psychophysical function, relating the perceived roughness, showed that twofold increase in the force resulted in 1.3-fold increase in perceived roughness

$$log R_{perceived} = 0.76 f_{lateral} - 0.51$$

where, $R_{perceived}$ is the perceived roughness and $f_{lateral}$ is the maximum lateral force.

A tactile display device - STReSS (Stimulator of Tactile Receptors by skin Stretch) was introduced by Pasquero and Hayward [PaHa03, Pasq03] based on the idea that lateral skin stretch can produce tactile sensations. They developed the system, STReSS, that provides an impression of skin indentation with active touch. The system is comprises of 100 piezoelectric actuators compactly arranged in a 1 cm^3 to provide a 1 kHz refreshing rate which is equivalent to the bandwidth of skin receptors. These piezoelectric actuators are driven by Programmable logic device (PLD) to supply the required voltage. Each actuator is capable of moving tangentially along the same axis which forms a deformable structure that can generate strain fields in the skin of the finger pad when comes in contact.

2.2 Haptic Texture Rendering

According to Laycock and Day, "the process of determining a reaction force for a given position of the haptic device is known as haptic rendering"[LaDa07]. Haptic interfaces employ rendering algorithms to compute force-feedback that effectively simulate the object characteristics to the perceiver. Haptic texture rendering conveys the sense of fine texture of object's surface. Rendering of surface texture with microscopic detail is one of the challenges in haptic rendering. The major role of texture rendering algorithms or systems in haptics is to present a perceptually realistic texture in the virtual environment. One of the commonly used algorithms in haptic rendering is to let the perceiver penetrate

the virtual object or model and feel the deformation of the object depending on the force applied. Traditional haptic rendering methods that calculate the feedback force typically differ in the way they compute the forces and render them.

The following gives an overview of the different haptic rendering methods that generate adequate force which can simulate the presence of a virtual object. One of the classical approaches in literature is penalty -based rendering [MRFV*96, ThSa 94]. In penalty based rendering approach, a restoring spring force is calculated proportional to the depth of penetration into the virtual object. However, this method suffers from severe drawbacks, as for instance, strong force discontinuities are evident while passing through edges of the object and limited volume constraints the generation of compelling forces for thin and small objects. These limitations have been addressed and overcome by Zilles and Salisbury [ZiSa94] who introduced a constrained based "god-object" algorithm. A virtual model named God Object is created to imitate the haptic interface point (HIP) in the virtual environment. In free space, the position of the HIP is same as the position of the god-object estimated by haptic encoders. On the other hand, when the HIP penetrates into an object, the position of the god-object is restricted to stay on the object's surface. The restricted god object position on the virtual object is chosen such that the distance between HIP and god object is minimized. Once the position of the god object is calculated, a simple second order spring-damper system can be assumed between HIP and god-object to compute the feedback force. Another constraint-based approach, "Force shading" has been developed by Morgenbesser [Morg95] and Ruspini et al. [RuKK97]. Force shading uses a similar concept to Phong shading [Phon75] in graphics. The concept behind this approach is to make use of the surface normal at a particular

point that is calculated based upon the vertices of the polygonal model of the object. Morgenbesser used surface normal information to alter the direction of haptic force while still retaining the magnitude of the force caused by the penetration depth of the original model. Ruspini et al. also introduced a configuration space obstacle model to efficiently estimate the position of the virtual proxy. This model ensures the stability of movement of the proxy provided that input from the user is stable.

In general, haptic rendering algorithms are classified into two categories based on contact interaction: point-based interaction and object-object interaction. The first category, point-based interaction, also known as 3-DOF haptics, captures fine-geometric details of an object. This class of haptic rendering which deals with tracking a textured surface with a single contact point follows an analogy of tracking a textured surface with a probe in real world. In the mid 1990s, Minsky [Mins95] developed the "lateral force gradient algorithm" for simulating haptic surface texture. She pioneered the concept of using only lateral (tangential) force to perceive the roughness of textured surface and developed the "Sandpaper" system with a 2-DOF joystick to allow the user feel textures. Her system was build around a spring force model that pull the user's hand towards low regions and away from high regions of a texture's height map. The texture forces proportional to the local vector gradient of the texture height map is calculated as

$$f_{texture} = k\frac{\Delta h}{\Delta x}$$

The initial hypothesis of her work was to claim that texture can be conveyed through tangential forces. This hypothesis served as base for many algorithms that were

developed later for texture rendering. Ho et al. [HoBS99] also suggested three dimensional texture forces by altering the magnitude and direction of the force based on the original surface normal and the local height field gradient, an approach similar to bump mapping [Blin78] in computer graphics.

Probabilistic approaches that leverage the statistical properties of the surface have been implemented successfully to render synthetically generated textures with 3-DOF contact forces. Siira and Pai [SiPa96] simulated various degrees of surface roughness for sliding contacts using a Gaussian distribution. The height of the surface is obtained by using a 2-DOF haptic interface. It was accomplished by sampling the implicit surface at points $v \times n \times dt$ where v is the velocity at which the haptic probe moves laterally along the surface, n is a random positive integer generated to represent the surface asperity[2], and dt is the sampling time period. Since the surface asperity value which is added to the sampled height is not dependent on velocity, it results in a Gaussian distribution. For a more realistic feel, they formulated the resultant force f_{result} as the summation of normal surface constraint force f_c, texture force f_t and friction forcef_f.

$$f_{result} = f_c + f_t + f_f$$

Fritz and Barner [FrBa96] extended the use of stochastic methods based on the vector perturbation method. They generated texture vectors by procedural methods on a uniformly spaced 3D lattice structure. They employed 3D lattice structure such that the texture information has no influence on the object shape. Generally, the stochastic

---

[2] Surface asperity is defined as surface irregularities that deviate from the normal.

methods or procedural methods use mathematical functions to generate synthetic haptic textures. Accordingly, they used probability density function (for example uniform, Laplacian, Gaussian etc.) to simulate real textures that are perceptually distinct from each other. They suggested that any qualitative texture is represented by spectral description such as periodicity, spectral power and frequency components. By manipulating the above spectral properties, the authors state that the qualitative descriptors of the surface texture could be altered. In other words, by modifying the variance of the Gaussian distribution, a broad range of surface textures that differ in roughness perception could be generated. One of the methods, namely "Implicit procedures and Fourier spectral synthesis", suggested by Fritz and Barner is to generate the texture vectors by using periodic functions. The texture force vector at any point $p, f_t(p)$, is computed as a combination of implicit and multiplicative noise given by

$$f_t(p) = Sg(p) + N$$

where $g(p)$ represents an implicit deterministic function that follows a periodic nature, S is a multiplicative noise and N represents additive noise.

Recently Nico. Galoppo et al. [GOMG*06] presented a novel technique to simulate the dynamic contact between deformable objects made of high-resolution surface geometry. Their main assumption was to represent the deformable object in terms of rigid core and the surface features as a deformable material layered on top of the core. The deformable surface is represented in 2D parametric atlases and a mapping is done from 3-dimensional deformations to a 2-dimensional parametric domain. This layered

representation of models with implicit formulation of dynamic motion and collision response let them decouple the elastic velocities with the core velocities in a highly simultaneous fashion. This approach is claimed as much faster to handle the dynamic contacts and collision detection with rich models compared to quasi-rigid dynamics system. Several researchers adopted well established techniques from the field of computer graphics to haptics [HoBS99]. One of the prominent ways of texturing 3D object in computer graphics is by wrapping a digital image around them to make them appeal more realistic. Basdogan et al. [BaCS97] introduced a classic approach of haptic texture rendering called Image-based haptic texturing. The idea is to create a texture height field from the image data. The texture height field is constructed from the grayscale intensity for each texel of a 2D image and mapped to the 3D object. They extended the two-stage texture mapping technique of Bier et al [BiSL86] and Wat et al [WaWa92] to map the 2D image data to the surface of 3D objects. After the mapping, corresponding texture coordinates are assigned to the vertex of the original object.

All the methods of haptic texturing which are discussed until now, i.e. point-based interaction, were implemented by either perturbing the surface normal or by manipulating the surface friction. A novel approach had been introduced by Laehyun Kim et al. [KKSD02] in haptic rendering by taking advantage of both geometric and implicit surface representations of the 3D object. This method also extends to representation of haptic surface textures. An implicit surface is defined for the external surface of the geometric model with a potential value with respect to the haptic tip position. A potential value of zero determines that point lies on the surface and a value of 1 or -1 indicates that

the point is outside or inside the surface. A volumetric representation, wrapped around the surface model, is used to store this signed potential value in a 3D rectangular grid. The potential value on the each cell of the grid determines its proximity to the surface. Any texture pattern is then mapped into the implicit surface by altering the geometry of the implicit surface rather than the original geometry which reduces the computation cost. As a result, the texture forces are computed dynamically and rendered through a haptic interface when the tip moves along the surface.

The second category, object-object interaction of haptic rendering is known as six-degree-of-freedom (6-DOF) haptics. For rendering the forces, which occur due to interaction of two geometric objects, the point-based techniques are inadmissible. A perceptually-inspired force model is proposed by Otaduy and Lin [OaLi04] which display the haptic texture information resulting from the interaction between the two textured surfaces. They developed their base idea from the concept of offset surface that is traced by the spherical probe during exploration on the surface texture in the absence of dynamic effects. If the spherical probe penetrates the surface, such that the center of the probe moves along the surface, then a vertical penetration depth is computed that is equivalent to the height of the offset surface. This concept is extended to describe the interaction between arbitrary surfaces by taking advantage of the contact normal that is calculated from the low resolution approximation of the surfaces. Once the directional penetration depth between two objects, δ, is known, a penalty based model, U, with stiffness k is applied to determine the textured force f.

$$\begin{pmatrix} f \\ t \end{pmatrix} = -\Delta U$$

where, $U = \frac{1}{2} k\delta^2$, Δ is the gradient in 6-DOF configuration space and t is the torque.

2.3 Reality Based Models for Vibrotactile Feedback

Reality based model for virtual environment is one where models are created using data acquired from real environments by employing various sensors [PLLW99]. Collecting data from physical environments and reproducing them in haptic environment is a tedious task due to complex dexterity of haptic feedback. One of the common approaches in acquiring physical properties of the real world object and integrating them to the virtual environment is through a sensor based approach. For example, Andrews and Lang [AnLa07] presented a cost effective system for modeling realistic textures. Their system consist of a haptic probe "WHaT", a pin hole camera and a tracker system that could track the position of the probe. The surface roughness of the object is estimated by scanning the object with the sensor that is capable of measuring force and acceleration. With the data acquired, a set of filtering and signal conditioning is performed to the data to remove the external noise. The surface profiles obtained from the scans are played back on to the virtual object to create a sense of realistic textures. A robotic based acquisition method is implemented by Pai et al. [PLLW99] to measure the real multimodal data such as contact texture, sound and deformation of the object. In this method, ACME, ACtive MEasurement facility, embedded with various sensors, is used to collect various physical measurements and to build realistic models.

In contrast to robotic sensor based methods, Kuchenbecker [Kuch08] proposed a haptography sensor suite that captures the mechanical properties of a material as well as information on user interaction such as position, orientation and muscular movement to

produce realistic haptic models from multi-sensory recordings. After recording the data a haptic distillation process is introduced to segregate the multi-sensory data into individual haptic interaction models, including geometric objects with their surface properties, that provides to build an enriched haptic library. They also suggested that the recorded data, inclusive user interaction information, can be recreated haptically by focusing on dynamics and band-width of the haptic interface.

The role of reality-based models in virtual environment was specifically addressed in vibrotactile feedback system. The vibrotactile feedback is gaining popularity in reality based virtual environments to increase realism. Early work on modeling the vibration waveforms and playing it back through the haptic interface was done by Wellman and Howe [WeHo95]. They used 5 different material samples that differed in their stiffness such as Polystyrene foam, RTV Silicone, Basswood, Plastic and Aluminum of *50 mm x 50 mm* with a thickness of *10 mm*. They observed a decaying sinusoidal vibration waveform when subjects tapped on the material surface with an aluminum stylus. These waveforms are then produced back to the subjects through a haptic interface, augmented with a voice coil motor. The results showed the effectiveness of the vibrotactile stimulation in conveying the stiffness information. The human ability to differentiate the stiffness of various surface in real and virtual environments was studied which showed that the virtual environments worked almost as well as the real ones. Their work demonstrated that high frequency vibrotactile feedback can effectively alter the way objects are perceived in virtual environment.

Okamura, et al. [OkDH98] extended the above vibrotactile model to a wider array of materials from tapping to puncturing membrane in medical training applications and stroking textures with a stylus. They measured the vibration waveform that resulted from tapping on real surfaces with a stylus. An exponentially decaying sinusoidal model was chosen as the empirical model to ft the vibration waveforms. The approximation is given by the equation

$$Q(t) = A(v)e^{-\beta t}\sin(2\omega t)$$

where the parameters, $A(v)$ attack amplitude, a function dependent on the impact velocity, β the decay constant of the sinusoidal waveform, and ω the frequency of the sinusoidal wave. All the above parameters depend upon the nature of the material sample. To create a realistic vibration feedback model, taking into consideration the bandwidths of the haptic display and human tactile sensitivity, a scaling is performed to the physically measured parameters. They used a 6 DOF desktop haptic device both to measure the vibration parameters in the real environment and to display back the vibration waveforms in a virtual environment. Their work showed that by accurately determining the vibration parameters, the vibration feedback model alone enhanced the realism in comparison without vibration feedback. Okamura et al. discussed the application of the vibration feedback model to the tactile task of stroking textures and puncturing a membrane. However, there is no vibration algorithm implemented for general textures such as sandpaper.

2.4 Summary

In this chapter, using literature studies, we highlighted the perceptual dimensions of an object that are considered more salient in haptic world. We analyzed different existing haptic rendering algorithms that are known to be effective in computing compelling feedback forces by haptic interfaces as the user navigates in the virtual environment. Algorithms that are employed for haptic textures to represent surface features are also briefly detailed. Reality-based modelling and implementation of it in different applications was also reviewed. From our analysis of reality based modelling, we summarize that by incorporating physical data, we add high-frequency details to virtual reality which increases the realism of the application.

Chapter 3: Background

The objective of this thesis is to introduce reality based vibration feedback texture to haptics that can provide tactile sensation to end users in a virtual environment. One of the requirements for accomplishing this objective is to collect texture from real world samples. Scanning of surface with stylus- based instruments to analyze the underlying texture of the surface is one of the widely used robust techniques for the accurate measurement of real textures. In collecting textures, we employ the scanning system developed by Andrews [Andr07]. Andrews, in his work, demonstrated a scanning system for acquiring surface texture and compliance of real-world objects. Since this thesis goal is partially related to Andrews's work, a brief discussion on Haptic Texturing system established by Andrews is portrayed in this chapter to provide the reader with some necessary background information.

3.1 Acquisition System

In this section, we discuss hardware components that are used to acquire the texture information from real world objects. A tactile probe, the WHaT (Wireless Haptic Texture Sensor) [PaRi03] is employed to collect the surface texture of the samples by scanning. The WHaT is a texture sensor designed to measure the magnitude of contact force and the acceleration between probe tip and surface when the probe moves along the surface of the object. Figure 4 shows the probe tip of the WHaT device. The device measures

acceleration in three directions and force along the major axis of WHaT at a rate of *500 Hz*. The WHaT is a wireless device and can transmit the sensor data over a RF link to a host computer with a low latency of *2ms* [PaRi 03]. During the texture scan, a registration of the trajectory followed by the WHaT relative to the currently scanned surface is required. Since the WHaT is capable of generating force and acceleration, a need for an estimation of the global position and orientation of the probe exits.

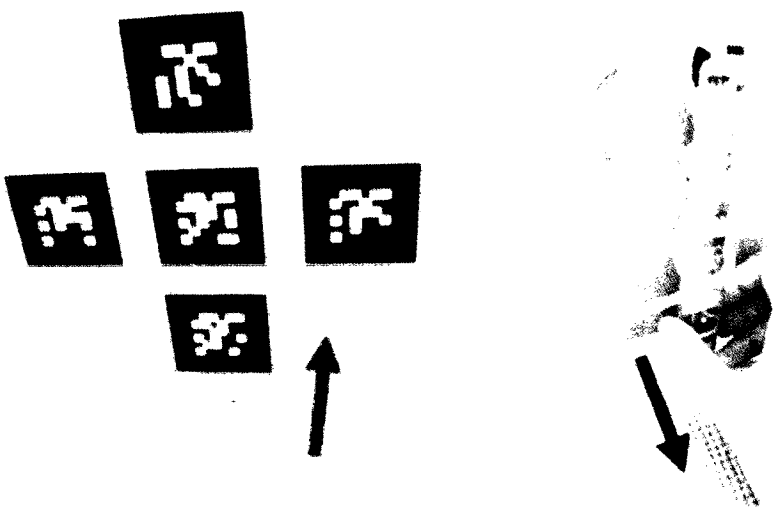

Figure 2: Scanning of a Rubber mat in the direction shown by arrows with the WHaT. The visual target is shown on the left.

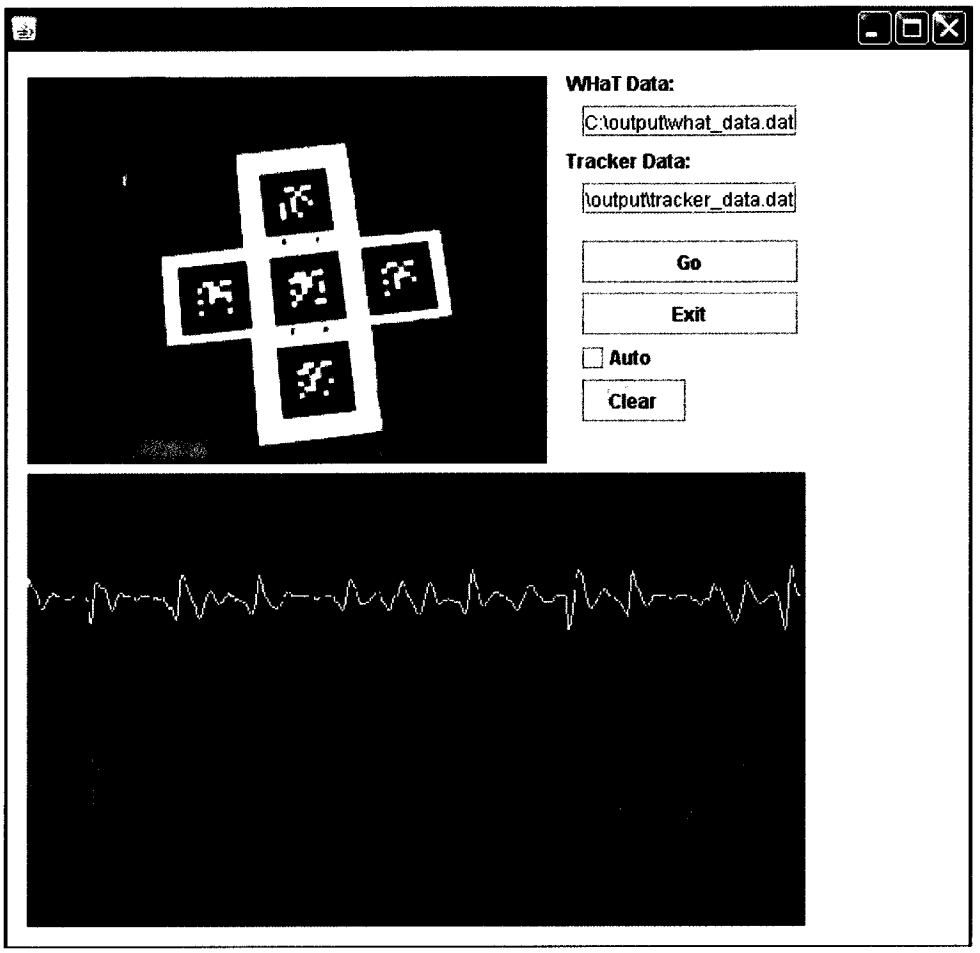

Figure 3 Scanning Application with ARToolkitPlus

To achieve this, a marker-based vision tracking system is employed. The task of visual tracking system is to recover the camera pose by consistently detecting a set of markers in each image of an input sequence. In this system, a Point Grey Dragonfly Express Camera is employed to capture the markers that are affixed in front of the probe. The camera is capable of capturing 640x480 full-frame color image at the rate of 200Hz [POINT GREY]. Initially ARTag [Fial04], an augmented reality system, was employed to recognize the markers within the camera images in Andrews' work [Andr07]. Now the system is upgraded to much faster speed using ARToolKitPlus [Wagn09]. It records the position and orientation information of the probe at an average rate of 85Hz ~ 100Hz,

which is faster than the previous system having an average rate of 45Hz. This gives a very high accurate trace of the probe within a scanning distance of roughly 300 to 600mm. Figure 3 depicts the scanning system with the markers affixed to the WHaT probe and force-acceleration profiles from the WHaT while stroking the surface textures.

Figure 4: Probe tip of the WHaT device

3.2 Data Acquisition and Signal Conditioning

The data from the sensors is noisy because of the wireless communication. It is important to have well-conditioned data in order to synthesize precise versions of textures. Some noisy data can simply be removed by thresholding but more advanced processing is required to get noise-free data. This sections talks about synchronization, filtering, and processing techniques to obtain a noise free sensor data from the raw sensor data.

Due to unsynchronized collection of data from the WHaT and the optical tracker, a synchronization step is required. The tracker traces the position and orientation of the probe at a rate of approximately 85Hz ~ 100Hz, whereas, the WHaT records force and acceleration values about the probe tip at a rate of 500Hz. By introducing a new time

series vector with a *1 ms* sampling period, the data from both the WHaT and the tracker are resampled and interpolated. This synchronizes the data successfully by providing a uniform sampling rate with the new time vector.

Once the synchronization step is achieved, the next phase is to filter the extraneous noise from the tracker data. In terms of accuracy, the calculated pose by most of the vision based camera tracking system is error prone. For the purpose of error minimization in the estimates, a good filtering technique is needed to remove the noise while retaining the useful information. A linear Kalman filter is employed for this task. A Kalman filter [CuZR05] estimates the states of a dynamic system from a series of noisy measurements. As the operator scans the surface of the object with the WHaT sensor, he/she holds the probe in an arbitrary orientations. To determine the pose of the probe with respect to the scanned surface, an acceleration blending technique is implemented. The surface profile of the object is generated based on the motion of the probe in the normal direction corresponding to the surface being scanned. The blending weights are obtained by calculating the dot product of the normal vectors along the scanning path with each of the unit-vectors of the axes of the sensor coordinate frame. A coordinate transform is required from sensor coordinate frame to world or camera coordinate frame. Finally, this acceleration is projected into the direction of the unit normal of the surface which results in an acceleration vector for each point on the filtered trajectory path of the probe.

3.3 Texture Synthesis

In this section, we discuss synthesizing textures from the processed sensor data. A surface profile is generated by interpolating the filtered acceleration data over the scan

path. These profiles are named as acceleration profiles to avoid ambiguity, as later discussions contain other profiles. Figure 2 portrays the scanning of a rubber mat with the WHaT by following the above described setup and Figure 5 shows the acceleration profile for the rubber mat.

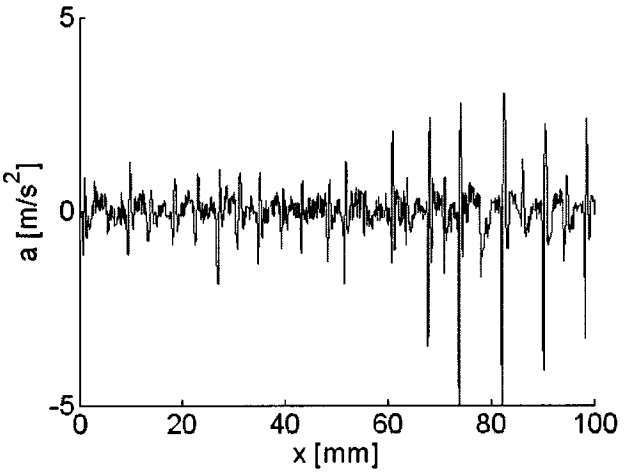

Figure 5 Acceleration Profile of rubber mat

In Andrews' work the height profile is employed, where in the profile represents the texture parameters of the scanned surface in terms of a height-displacement relationship. A Verlet integration method [Verl67] is used to generate a height profile, h, from the acceleration data. Mathematically, with the acceleration data and for small time step Δt, the Verlet algorithm estimates the height at the next time step, h_{i+1}, by calculating the height at the previous time step, h_{i-1}, and current time step, h_i.

$$h_{i+1} = 2\,h_i - h_{i-1} + |s_i a_{n,i}|\Delta t$$

3.4 Compliance

Compliance can be defined as material characteristic of the object which is estimated in terms of a force-displacement relationship. It can be described as the amount of displacement undergone by an object from its original surface structure when an adequate force is applied. Various external devices or apparatus are used to measure the compliance. In the system developed by Andrews, compliance is computed by taking advantage of force acceleration profiles from the WHaT. A compliance estimate, k_c, is determined statistically by measuring the variance, σ_r^2, of the force acceleration profile. The value of k_c varies from 0~1 where 0 indicates a soft surface and 1 indicates a stiff surface. The computed compliance estimate, k_c, can be stated by Andrews's equation:

$$k_c = \frac{1}{e^{\sigma_r^2}}$$

In our work, we estimate compliance by fitting an experimental relationship between force and acceleration which was observed by analyzing the influence of force on acceleration values. A detailed discussion of our compliance estimation approach is presented in chapter 5. Outcomes of our approach are addressed in chapter 6.

3.5 Texture coordinates

In computer graphics, the process of applying a surface texture to a 3D object is known as texture mapping [SAGM*05]. In texture mapping, an image or a texture is mapped around the 3D object by creating a mapping, or correlation, between coordinates in the object space and coordinates in the texture space. Similarly, a texture painting method is defined in order to apply the approximated surface profiles to a virtual 3D object.

Applying the height profile to a 3D virtual object comprising a set of polygons require registration of the scanning trajectory with the 3D geometry of the object and generation of 2D texture coordinates on the surface of 3D object.

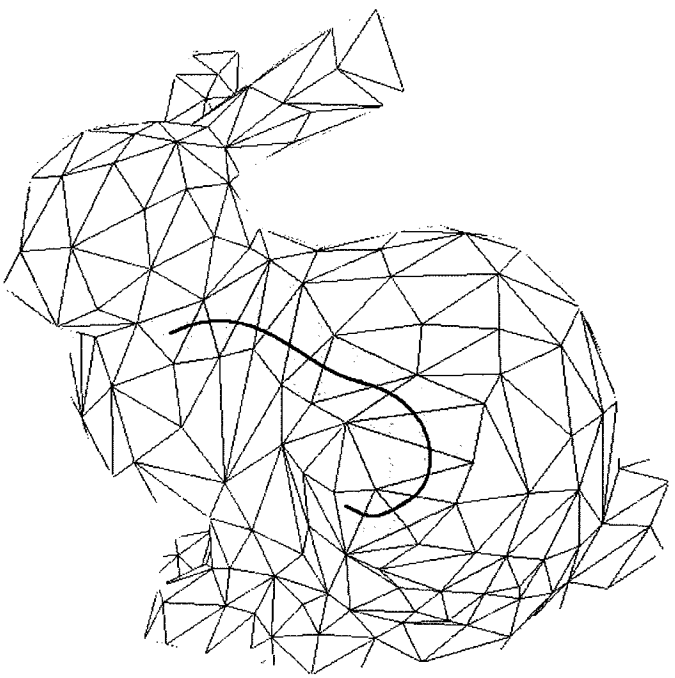

Figure 6 Superimposition of scan path on polygonal mesh. The bunny model is provided courtesy of MPII by the AIM@SHAPE Shape Repository

In registration of the texture with the 3D geometry, the points from the scanning trajectory are mapped to a polygonal mesh using an ICP (Iterative closest point) algorithm. The polygons which are overlapped by the scan path are associated with a texture coordinate. The texture coordinates are assigned to each vertex of the polygons. Figure 6 portrays a bunny with a scan path from the WHaT superimposed on a polygonal mesh with the relevant polygons shaded. The texture coordinates for particular vertex are computed as a function of x and y with respect to the mesh coordinate frame. To

determine the y value of a texture coordinate of a vertex a perpendicular line from the vertex is drawn on the scanned path. Assume that the line intersects the scanned path at point P. The distance between the vertex and point P is set as the value of y. On the other hand, the x value of a texture coordinate of a vertex is calculated by finding the distance between the initial point of the scanned path and point P. Figure 7 illustrates the texture estimation process.

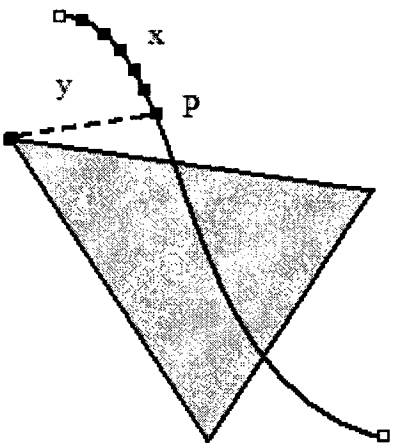

Figure 7 Texture coordinate estimation showing calculation of x-coordinate along the trajectory of scan path, whereas, y-coordinate is normal to the trajectory.

3.6 Haptic Rendering

Rendering texture based models in haptics is one of the challenging tasks due to the complexity of synchronization between haptics and graphics components. The estimation of the forces that leads to the perception of texture plays a vital role in haptic based application. The methodology incorporated by Andrews for haptic rendering is similar to the one used by Siira and Pai [SiPa96] and haptic texture is described in terms of forces

between the surfaces of the bodies in contact. The total force, F_t rendered to the user is given by

$$F_t = f_c + f_f + f_t$$

Here f_c and f_t are normal force and f_f is the tangential force. Each force component in the force equation has a significant addition towards the model of the surface texture in general. The force due to rigid body constraint, f_c, creates a virtual illusion of the rigidness of the surface by producing forces which oppose the penetration, Δx, between the haptic proxy and a 3D model,

$$\vec{f_c} = -k_s \Delta x \vec{n} \text{ , where } \vec{n} \text{ is the surface normal.}$$

The frictional force component f_f acts as counterattack to the tangential motion $\vec{t}$ and is proportional to the normal force to produce a frictional surface effect.

$$\vec{f_f} = -\mu_s |\vec{f_c} + \vec{f_t}| \vec{t}$$

Here, normal force is the sum of all forces acting in normal direction ($f_c + f_t$). Thus, rigid body constraint force and frictional force constitute the material property of the surface object.

The last component f_t, is the resultant of the texture force that is computed by the variation of the height profile, Δh. The texture force provides a sensation of surface roughness.

$$\vec{f_t} = -k_c k_s \Delta h \vec{n}$$

For haptic rendering of our vibrotactile texture model, we integrate a scaled acceleration profile into the texture force, f_t, rather than height profile, Δh. The scaled acceleration

profile is obtained from IIR filter. We provide an in depth analysis of computing texture forces integrated with IIR filter in chapter 6.

In Andrews work, the synthesized textures are represented by Fourier series. For each surface profile, a discrete Fourier transform has been applied to find the Fourier coefficients. Hence, the resulting texture can be expressed in terms of its composite harmonics as follows:

$$f(x) = \sum_{j=1}^{N} a_j \cos(j\omega x) + b_j \sin(j\omega x)$$

where x is spatial coordinate, a and b are real and imaginary parts of the DFT coefficients respectively. ω is the fundamental spatial frequency of the texture sample.

3.7 Summary

In this chapter we explain an existing mobile scanning system developed by Andrews. With the aid of his system, we measure the surface attributes – texture and compliance from real world objects. We also discuss his work on synthesizing texture based on height profiles and estimating compliance by measuring the variance of force-acceleration values. Our texture model in this thesis is developed by using acceleration profiles that are obtained directly by scanning surface of the object rather than deriving height profiles. We estimate the contact stiffness by scanning the surface with varying forces and approximating the relation between applied force and acceleration.

Chapter 4: Haptic Vibration Texture

Part of this chapter is reprinted with permission, from IEEE Int. Workshop on Haptic Audio-Visual Environments and Games (HAVE'09), Modelling of Haptic Vibration Textures with Infinite-Impulse-Response Filters, Vijaya L. Guruswamy, Jochen Lang and WonSook Lee.

Building realistic haptic textures for virtual reality applications from the data collected from physical environment can be a quite tedious task. To achieve this, we employed vibration feedback models that are known to be effective in providing tactile sensation. This chapter illustrates how we achieve vibration based reality models based on the impulse response of IIR filter for haptic texturing. Section 4.1 explains the idea behind our model. Section 4.2 talks about IIR filter in general and its characteristics. We present our IIR-filter based haptic texture model in Section 4.3 and detail the estimation of IIR filter parameters for our measured acceleration profiles.

4.1 Vibrations on Texture Stroke

We design our haptic texture model based on the force-acceleration profiles (see Figure 5) observed in scanning surface with the WHaT. Our intent is to explore the vibrotactile textures to all the surfaces irrespective of their characteristics, i.e., textures ranging from irregular pattern, like sandpaper, to a regular fashioned pattern.

When a surface is scanned with the probe, an acceleration pulse occurs at locations of peaks and dips in the surface. A positive pulse is generated when the probe runs over a peak in the surface, whereas a negative pulse occurs when the probe falls into a dip. These pulses portray the texture features of the surface being scanned. Inspired by Okamura et al. [OkDH98], we model such a pulse as the initial peak of a decaying vibration wave, i.e., the feature triggers a vibration at a certain location on the surface which then diminishes over time. Figure 8 and Figure 9 shows a synthetic example of our interpretation of such a haptic texture model with the Figure 8 depicting a distribution of collected pulses that are triggered by traversing the surface features and Figure 9 shows the corresponding vibration based acceleration profile when the surface is traversed with constant speed. Mention to be made that pulses are located in space whereas the decaying vibration waveforms that are triggered by the pulses are in time domain.

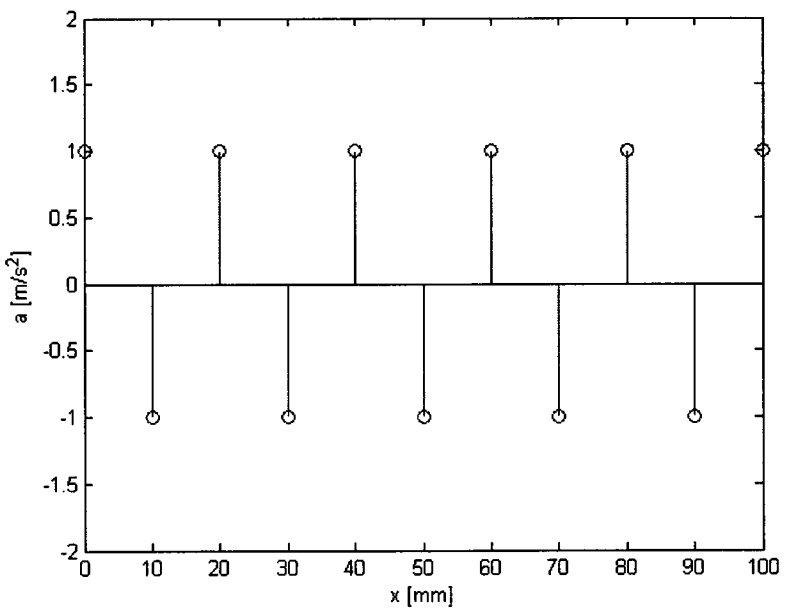

Figure 8 Filters locations in space due to surface feature.

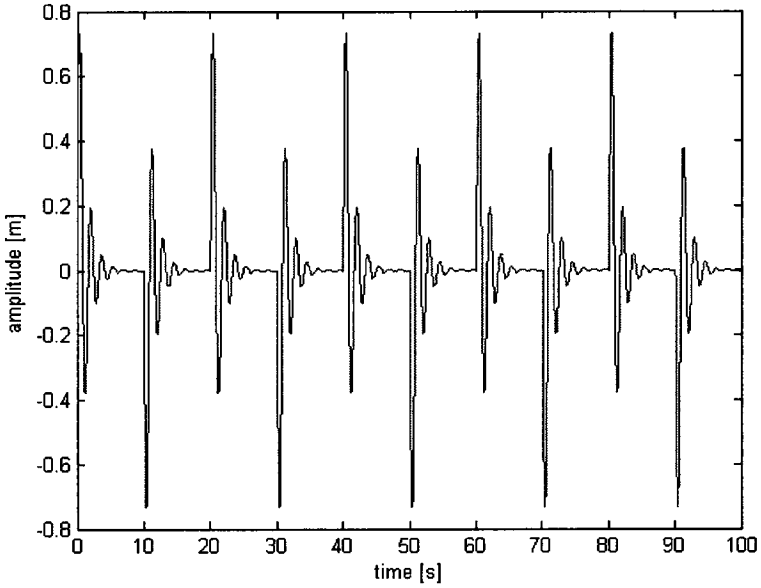

Figure 9 Filter responses damping in time with constant velocity.

Okamura et al.'s vibrotactile model used an exponentially decaying sinusoid given by the following equation:

$$y(t) = Ae^{-\beta t}\ sin\ \omega t \qquad (1)$$

Equation (1) is employed as an empirical model to approximate the vibrations obtained during stroking textures. Here, A, β and $f = \omega/2/\pi$ represent the amplitude, the decay rate and the frequency of the wave form respectively. We view the decaying sinusoid as the impulse response of a linear shift-invariant system. Instead of using a decaying sinusoid to model the acceleration response normal to the surface as the probe moves across it, we choose to use an infinite-impulse-filter (IIR) to model the vibrations. We deploy an IIR filter at each pulse location as shown in Figure 8 to generate the vibration waveforms. The IIR filter generates the decaying impulse responses in time at the feature locations in space. In the work of Okamura et al., haptic textures are classified as either

"general" or "patterned". General textures are basically stochastic without any discernible features, for example sandpaper, fibre cloths, while patterned textures have regular distinguishable features, for example ridges and grooves. Okamura et al. fit the decaying sinusoidal to the acceleration profile in the time domain in the case of patterned textures. However, they did not consider their model for general textures. We develop a novel unified filtering method for both, general and patterned, surfaces. In particular, we claim that stochastic textures are simply a collection of many low amplitude impulse responses at high spatial frequency. Thus, our unified model is applicable to any general surface ranging from stochastic to pattern. With the aid of IIR filter we model haptic vibration textures and render with low latency by taking advantage of its computational benefit.

We give a general overview on how IIR filters works followed by detailed discussion on how we model our vibrotactile textures with discrete IIR filter in the following sections.

4.2 IIR Filter

An IIR is a digital filter whose impulse response is infinite i.e., when an impulse signal (a pulse of one followed by zero) is fed to the filter, the output of the filter is not time limited.

The filter is defined recursively [PaLa97] as

$$y(n) = \sum_{j=0}^{M} b_j\, x(n-j) - \sum_{i=1}^{N} a_i y(n-i) \qquad (2)$$

where N $(N \geq M)$ represents the order of the filter, and b_j, a_i represent the coefficients of the filter, which determines the filter characteristics. The output, $y(n)$, of the IIR filter

resulted from weighted sum of current and past inputs, $x(n)$, and past outputs. The above Equation (2) can be re-written in terms of Z -transform to represent the discrete-form of IIR filter as follows:

$$H(z) = \frac{Y(z)}{X(z)} = \frac{\sum_{k=0}^{M} b_k Z^{-k}}{1 + \sum_{k=1}^{N} a_k Z^{-k}} \tag{3}$$

Figure 10 shows the cascade design of IIR filter with respect to Equation (3). IIR filters have a computational benefit over finite-impulse response filters. Since filtering in IIR depends on the feedback path, computationally feedback subtraction equals to summation with inverted coefficient values without an overhead on additional arithmetic.

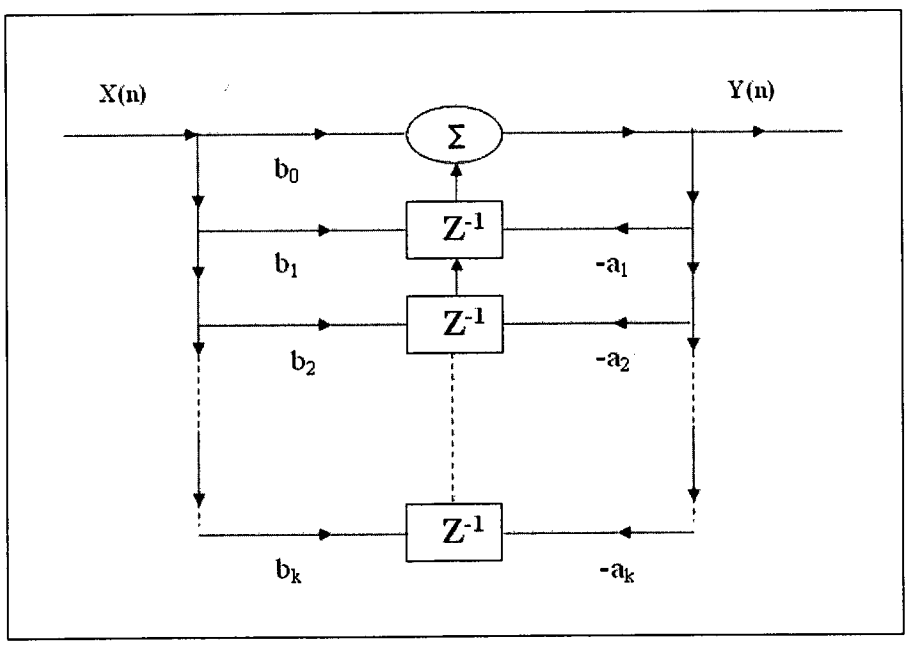

Figure 10 IIR Filter Structure with order $N = M = k$

The most important advantage of the IIR filter model for haptic textures is its ability to have a large range of different frequency response. We leverage this characteristic of

the IIR filter to model richer vibration waveforms based on our measurements of acceleration-force profiles.

4.3 Vibration Texture Model via IIR Filter

This section describes the procedure of designing a set of space-sequential IIR filters with a combined impulse response that approximates the acceleration profile over time. We proceed by segmenting the entire acceleration profile into individual segments which have decaying waveform characteristics. We interpret the individual segments as the impulse response from a single filter and find the corresponding IIR filter coefficients with Prony's method [PaBu87]. We explain the procedure by first considering a single segment of the acceleration profile that follows a decaying waveform pattern and extend our approach for the entire acceleration profile by introducing a segmentation method. The procedure is carried out by fitting a decaying sinusoidal model given by Okamura et al. through our IIR filter followed by designing a high order filter that can effectively approximate the acceleration profile acquired by real world samples. The single segment of the acceleration profile is extracted from the entire profile is shown by dotted curve in Figure 11. The segment's start and endpoints have been selected such that the absolute heights of the local extrema are decreasing, i.e., the overall acceleration wave is of decaying nature.

4.3.1 Decaying Sinusoid Model with IIR

Following by Okamura et al, we fit a decaying sinusoid to the acceleration wave shown in Figure 11 through impulse response of the IIR filter. Assuming that the vibration can be described by a decaying sinusoid as Equation (1)

The corresponding IIR filter's Z-transform equation is given by

$$H(z) = \frac{ze^{-\beta t}\sin \omega t}{z^2 - 2ze^{-\beta t}\cos(\omega t) + e^{-2\beta t}} \tag{4}$$

The above equation uses a discrete form of the filter with sampling time T. The parameters for Equation (2) are calculated by identifying the dominant frequency f of the waveform in the power spectrum of the acceleration profile. The dominant frequency is set as the frequency f of the sinusoid for the decaying sinusoid model of Equation (2). The amplitude A of the wave is approximated as the height of the first signed peak. We find the decay rate β by fitting an exponential to the absolute heights of the peaks in the segment. The resultant output from the IIR filter is shown by solid lined curve in Figure 11. While the decaying sinusoid describes the overall nature of the wave, the fit is quite poor.

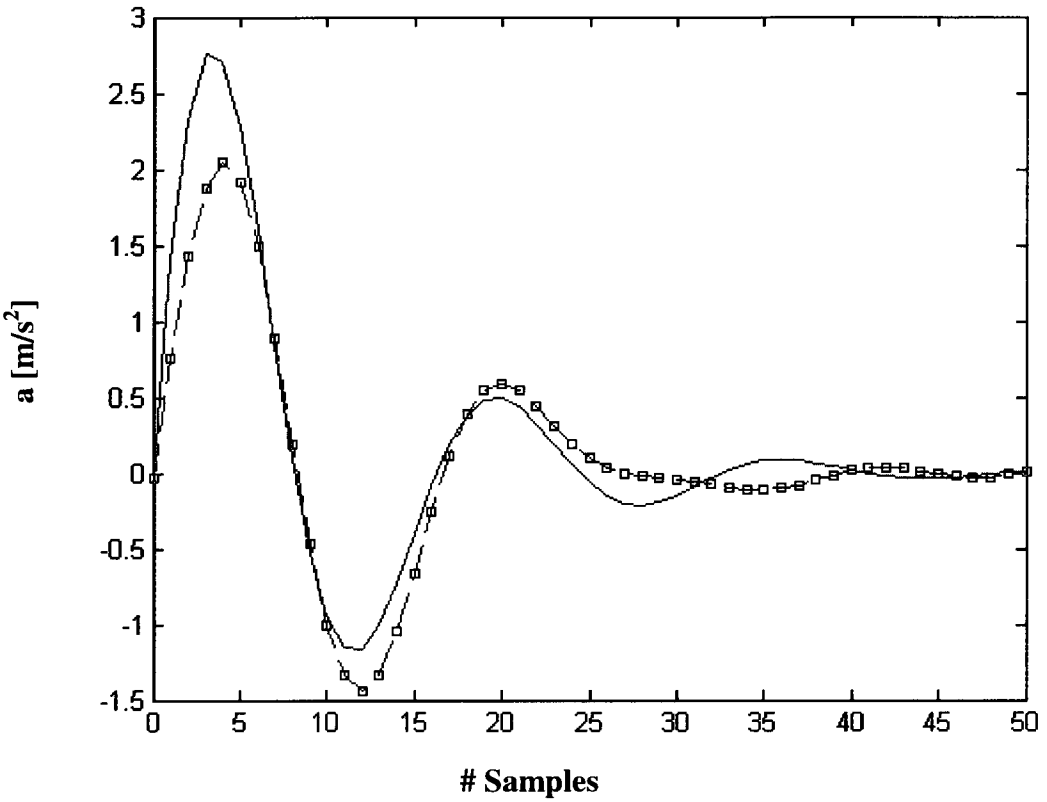

Figure 11 Estimation of decaying sinusoidal through IIR Filter. Dotted curve represents the measurements while solid curve shows the filter response

4.3.2 Vibration through Prony's Series

A closer fitting impulse response can be achieved by using higher order IIR filters rather than simply applying Equation (4) which is a discrete form of second order filter with a simple mass-spring damper system. We employ Prony's method to design such higher order filters based on our acceleration data. Prony's method is a time domain method for calculation of the filter coefficients based on the desired impulse response of the filter. The Prony's series estimates the filter coefficients of the desired impulse response by fitting a sum of damped complex exponential signals. Hence the series is a natural

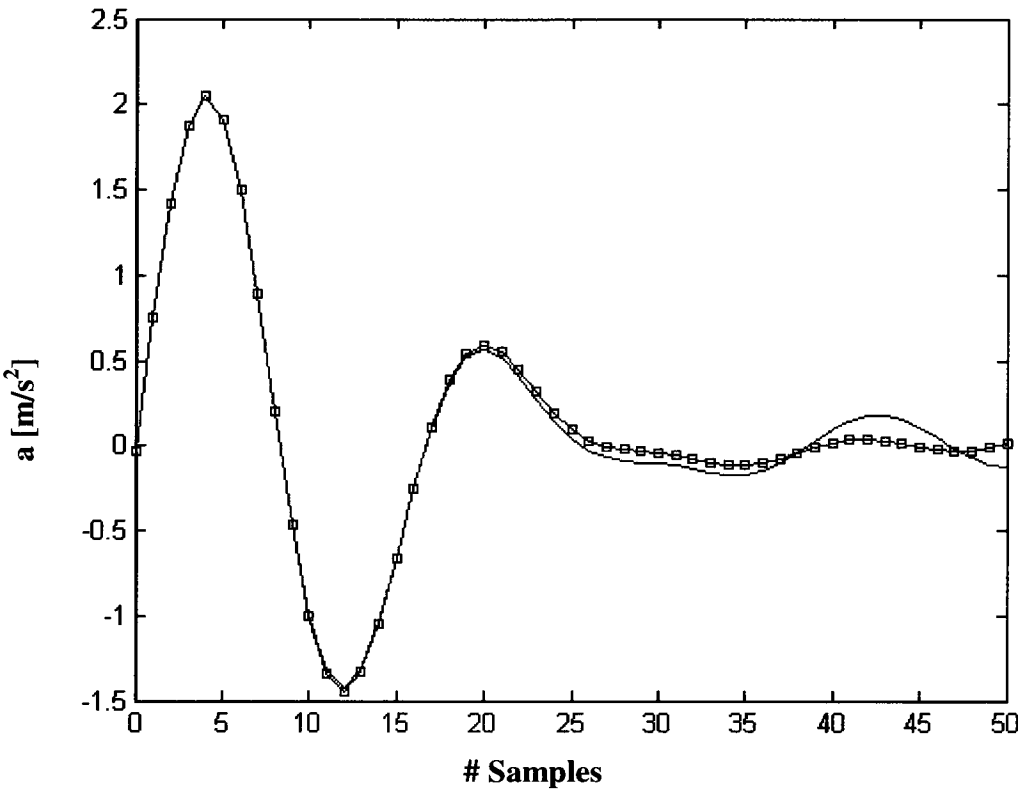

Figure 12 Estimation of IIR filter using Prony's Method. Dotted line represents the measurements and a solid line that approximates the dotted curve exactly represent the filter responses for N = M = 8 and the dotted curve which loosely fits the data is filter responses for N = M = 5respectively.

4.3.3 Segmentation of the Profile

In Section 4.3, we have assumed the existence of a segment of the acceleration profile in time with a decaying wave while defining a segment as an individual section of the profile where the absolute heights of the local extrema are decreasing. The acceleration profiles (see Figure 5) contain however many maxima which are larger than the earlier maximum. But if the IIR filter is to model the acceleration response to surface features, then the magnitude of its impulse-response should approach zero a short time after the

surface feature has been stroked. It is therefore reasonable to assume that each maximum with a higher magnitude than its predecessor is due to a different surface feature from its predecessor. This assumption is also consistent with the decaying sinusoid model. Our segmentation of the profile exploits this assumption and splits the acceleration profile into sections such that the absolute magnitudes of the local extrema are decreasing. Figure 13 gives an example of our segmentation process. We find the local extrema of the absolute value of the acceleration profile. The maxima will be the extrema of the signal and since the acceleration profiles are zero- centered, the minima are the start and end locations of a peak. The minima locations determine the extent of a segment since each segment extends between the two absolute minima preceding the respective sections' absolute maximum. Searching for extrema in a noisy signal will lead to many false positives and would result in an over-segmentation of the profile. It is therefore necessary to apply a filter to the signal first. In order to ease the IIR filter estimation process, we employ a bandpass filter with cutoff frequencies selected based on the power spectrum of the acceleration signal. The cutoff frequencies are found automatically by low-pass filtering the spectrum and then finding its critical points. The bandpass of the filter is set to frequencies between the minima surrounding the global maximum.

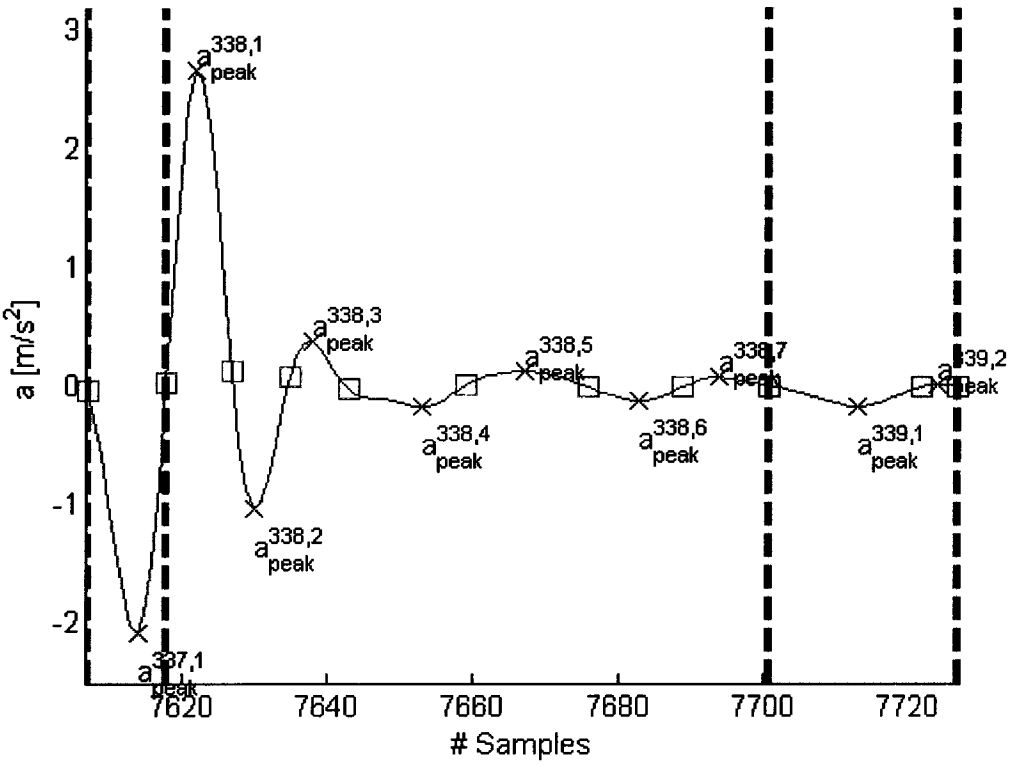

Figure 13: Segmentation of acceleration profile. The result of segment 338 of jewel case is presented here. Here $|a^{i,1}{}_{peak}| > |a^{i-1,j_{max}}{}_{peak}|$ and that $|a^{i,j}{}_{peak}| < |a^{i,j+1}{}_{peak}|$ where i is the i^{th} Segment in the profile and j is j^{th} absolute maximum within a segment. Here segment 337 has only one peak, $|a^{337,1}{}_{peak}|$, and the absolute value is smaller than the peak, $|a^{338,1}{}_{peak}|$, of the segment 338

Our IIR filter models fits the segments of profiles assuming the scanning velocity of the surface is scanned equal to the rendering speed of the profile. However, if the user traverses the profile with different scanning speed, the rendering profile somehow needs to incorporate this information so that the user feels seamlessly negligible perceptual difference. Currently our model assumes there is no influence of user's traversing speed on the scanning.

4.4 Summary

In this section we explained our reality-based approach to model vibrotactile texture through IIR filter. The ability of an IIR filter to have a large range of different frequency response facilitates us to model richer vibration waveforms based on our measurements of acceleration-force profiles. We also highlighted how our model fits the acceleration profile in time domain compared to decaying sinusoidal model of Okamura et al.. We give an overview of our design for IIR filter using Prony's method. We discuss further on results obtained from our vibrotactile texture model in chapter 6.

Chapter 5: Compliance

5.1 Compliance Overview

"Compliance represents the force-displacement relationship of a deformable surface and is the inverse of stiffness" [AnLj07]. Experimental studies on measuring the force-displacement ratio to calculate stiffness of material has been done by researchers [MaHa04][OkCD01][PDJL*01] in the haptics framework. In general, specimen (object under test) is probed with a force sensor. The maximum displacement undergone by the specimen from its original shape and the applied force are used as parameters to estimate the compliance. This method of estimating the compliance through force-displacement ratio is not feasible with the WHaT for two main reasons. First, WHaT restricts us from applying limited ranges of force by its piezoresistive force sensor. Second, since WHaT device is mainly designed to measure small scale motion, the accuracy of displacement derived from acceleration measurement with WHaT device is narrow. Due to these practical limitations, a statistical approach [LaAn09] is employed to estimate compliance of an object from the measurement with the WHaT. We conducted experiments on various objects ranging from hard to soft. Even though there exist several devices that give the direct measurement of force-displacement, the factor that motivated us in choosing WHaT to estimate the compliance of the object is cost effectiveness of the WHaT sensor. Considering structure and weight of the WHaT, it is more convenient to

handle compared to other relative devices. In addition, in our experiment we used the data from the WHaT to estimate both texture and compliance of the material. So, the data is consistent for the measurement as it comes from the sensor. Moreover, WHaT is a versatile device which can be easily extended to other parameters. An experimental observation is carried between acceleration and force of the WHaT while scanning surface of the specimen with varying applied force.

5.2 Dependency of Acceleration on Force

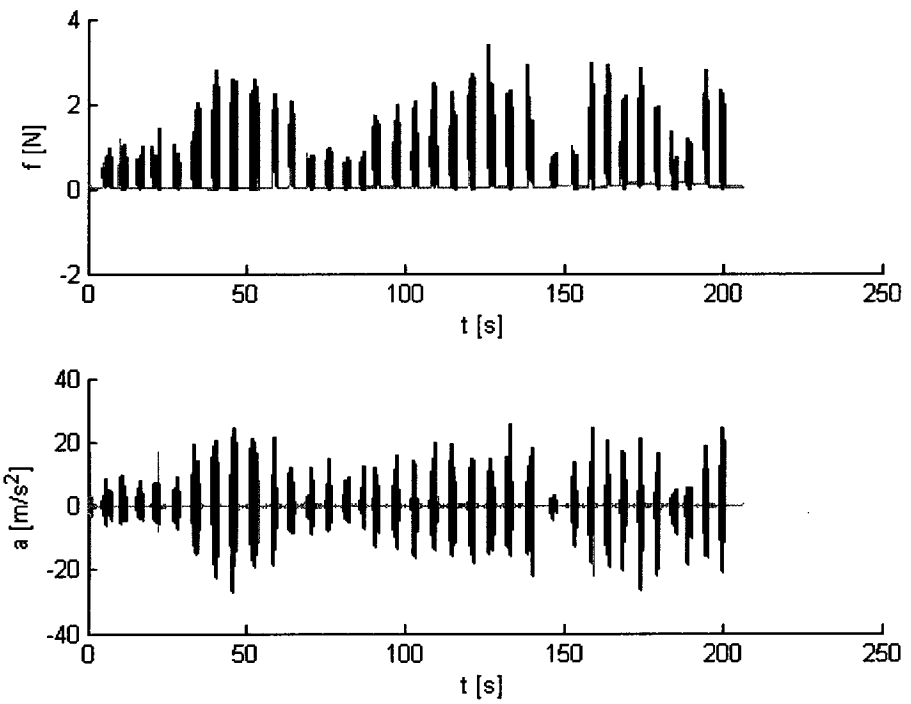

Figure 14 Influence of applied force on acceleration sensing while a user repeatedly scans (about 35 times) the surface of an object with different applied forces. The force shown is the force measured by the sensor which is proportional to the applied force

The Figure 14 shows force and acceleration values when the user scans the stiff cork object (show in Figure 43) multiple times with varying applied force. A proportional

behavior is observed in the measured acceleration values with respect to the measured force which in turn dependent on the applied force. This could be elaborated as: when the applied force is high, the amplitude of the acceleration goes high. On the other hand, when the applied force is low, the amplitude of the acceleration is attenuated. Here the average speed the user traverses over the surface is considered constant. Figure 14 clearly depicts the relation between force and accelerations. The higher the force is, the higher the acceleration.

Lang and Andrew [LaAn09] related this empirical relation to a theoretical concept by taking into account a second order linear dynamic system

$$m\ddot{u} + b\dot{u} + ku = f_{ext} \tag{5}$$

with stiffness k, damping b, mass m, displacement u and external force f_{ext}.

5.2.1 Generation of a combined profile

Since the user scans the surface multiple times, the user lifts the probe from one scan to the other scan indicating that the probe is on the air. This data recorded in our experiment does not correspond to any material characteristics. So, we need to cut out the sessions of the data where the force sensor does not record any force or the acceleration is under threshold suggesting that the probe is on the air.

We devised a simple fragmentation routine which cuts out sessions of the data from the measured data of the object. For example, the data shown in Figure 14 has 35 sessions and between each session, the probe was on the air. We aim to create a continuous profile

by combining all sessions after removing data, where the probe was on the air, from each session.

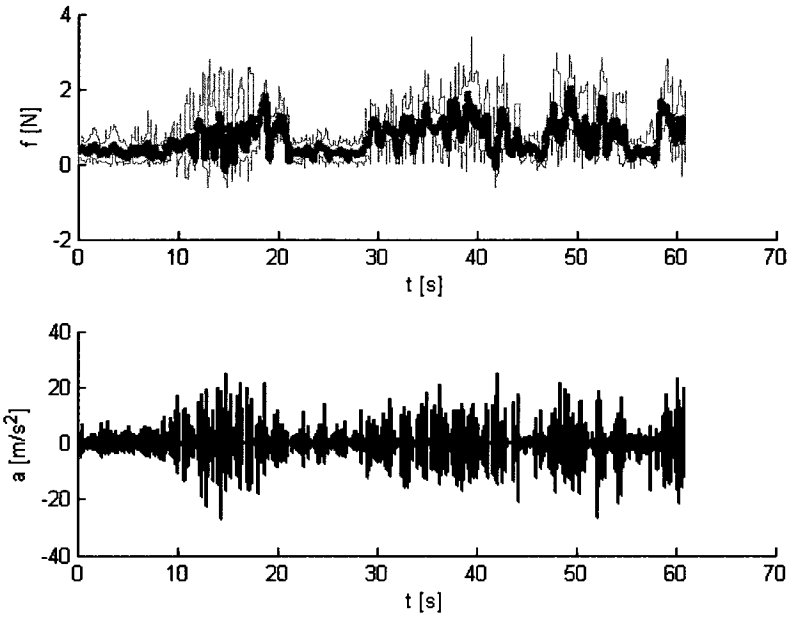

Figure 15: Combined profile after removing sessions of data, where the probe was on air, for repeated scans of cork. In the upper image, the thick line (brown bolded line) shows the low-pass filtered fore and the light line (grey colored) shows the original force. The lower image depicts the acceleration.

In the fragmentation routine, we first find where the force sensor is in contact with the object. We estimate a threshold value that determines whether the acceleration is low enough for the probe to be on air. We find the start of the session by comparing force and acceleration with the threshold. We pass the acceleration through a filter to remove the drift so as to allow calculation of minimal motion. If force and acceleration of the probe is greater than the threshold value and the motion of the probe is higher than minimal motion then the routine considers that the probe is moving. The continuous profile is as shown in Figure 15 for the input data shown in Figure 14.

5.2.2 Statistical Approach

A statistical approach is carried by Lang and Andrew [LaAn09] to estimate the compliance from the experimental analysis observed with the force and accelerations values from the WHaT. A plot of root-mean-squared (RMS) acceleration versus the lowpass filtered force gives a linear correlation that elucidates more statistically about the relationship between applied force and the corresponding acceleration. Figure 16 shows the plot of RMS acceleration over lowpass filtered force for the cork object. The lower image of Figure 16 portrays the RMS acceleration, while the upper image represents the force. A low pass filter is chosen to calculate a relatively proportional force to the average applied force by the user. In our experiments, a first-order Butterworth filter with a cutoff frequency of 2.5Hz is implemented. The RMS acceleration, a_{RMS}, gives the equivalent quantity of acceleration that occurred due to the external force and is given by the following equation:

$$a_{RMS} = \sqrt{\frac{1}{N}\sum_i a_i^2}$$

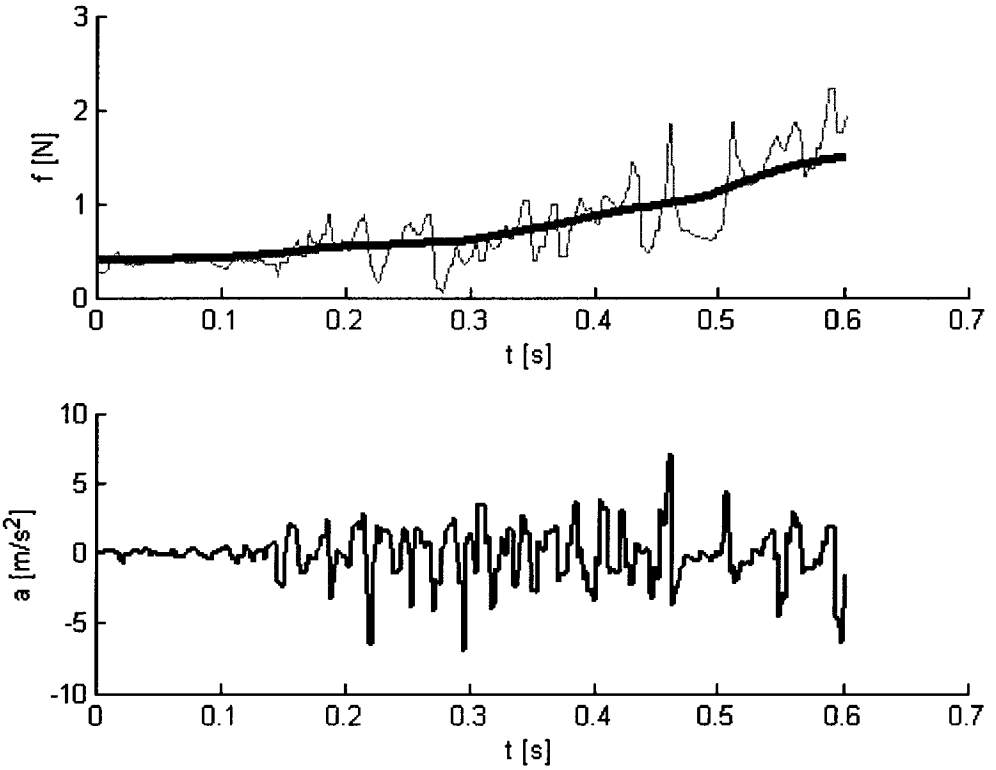

Figure 16 Force and acceleration for a single scan of cork. Top plot shows the measured force (grey, light) and low-pass filtered force (brown, bold) used for surface compliance estimation. The user applied force increases with time (from left to right). The bottom plot shows the RMS acceleration (blue, bold) .

The data from the sessions are partition into 24 bins down the force dimension. The bins are of equal size. Then we smooth the data by calculating the variance, $\bar{a}_j^2$, and mean, $\bar{f}_j$,values for acceleration and force for all the bins j. A weighted linear least squares regression is used to fit these variance and mean values from the measurement with weights as the inverse of the standard deviation, σ_j, of the acceleration for each bin given by the following equation

$$w_j = {}^1/_{\sigma_j}$$

The standard deviation of acceleration is given by

$$\sigma_j = \sum \frac{a_{i,j} - \bar{a}_j}{N_j - 1}$$

The equation of the line that fits the RMS acceleration and force which gives the linearity between them through a linear coefficient k_c is given by

$$a_{RMS} = a + k_c[\frac{1}{k_g} * (f_{lowpass} - \bar{f})] \quad (6)$$

An error bar indicating the standard error at the measurement of acceleration is also estimated.

5.3 Compliance Estimation

Statistically, the surface compliance is estimated by analyzing the relation between varying force and the corresponding acceleration values. The result of the line fitting for the data of the cork shown in Figure 16 is found in Figure 17 with stiffness coefficient, k_c, of 0.853 with a fitting standard deviation, σ, of 0.257. The observation from real world materials is that the ability to absorb an impact increases with the softness of the material. In other words, the vibrations caused on hard surfaces while tapping are high comparatively to the vibrations caused on softer material. The softer materials tend to absorb the impact from tapping. This argument is supported by solving the second order system of Equation (5), for the damping ratio, ζ, by considering a simple Rayleigh damping with damping coefficient $b = \alpha m$, leads to

$$\zeta = \frac{\alpha}{2}\sqrt{\frac{m}{k}}$$

The damping ratio as shown by the above equation is inversely proportional to the square-root of the stiffness k. So, we tend to see higher damping for less compliant surfaces i.e., accelerations decay more rapidly with the increase in the k_c value.

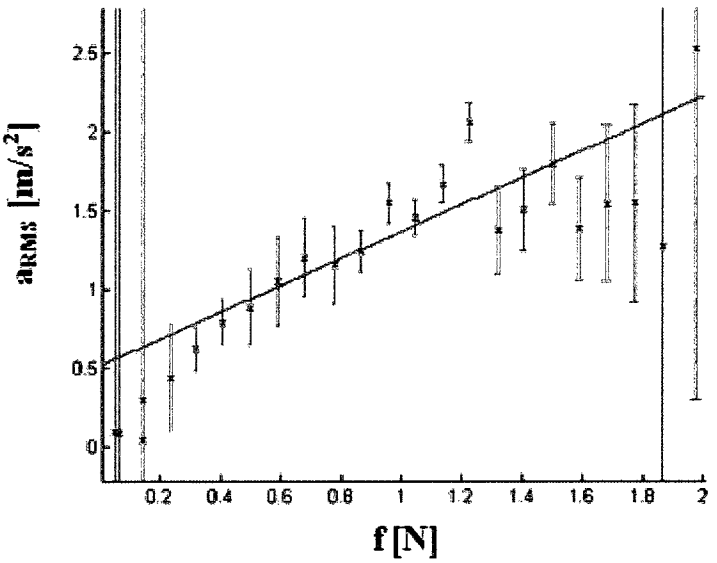

Figure 17: Linear approximation of the dependency of acceleration on force for cork with error bars

By fitting the line through measurements as discussed in the section 5.2.2, a linear coefficient proportional to the force and acceleration is estimated which is the compliance coefficient k_c of material surface. However, we noticed two behaviors while scanning the surfaces with different amount of force. First, the estimation technique is relied on surface roughness, i.e., according to Lang and Andrew "completely smooth surfaces will exhibit only very small accelerations no matter what force is applied." Consequently, surfaces with no features (smooth surfaces) are not adaptable in this approach of compliance estimation. Second, by observing the standard deviation of fit with respect to stiffness estimates we found that some objects with irregular molecular cell structures, especially foam objects, do not comply well with the line fit. For example, the Figure 18,

Figure 19 and Figure 20 shows the line fit for Rubber tire, Foam A and Toy (foam) with linear coefficients of 0.526, 0.115 and 0.157 respectively. But the standard deviation of fit is quite high for Foam A,[0.310] and Toy (foam),[0.102] compared to the rubber tire, [0.096]. This is because the three objects differ in their internal cell structure. We analyze the reason for the variation of stiffness by observing the standard deviation of fit.

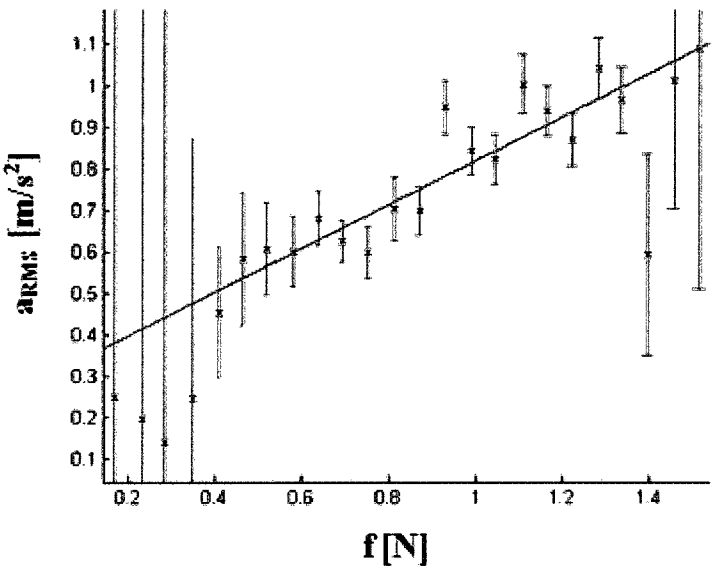

Figure 18: Linear approximation of the dependency of acceleration on force for Rubber tire with error bars.

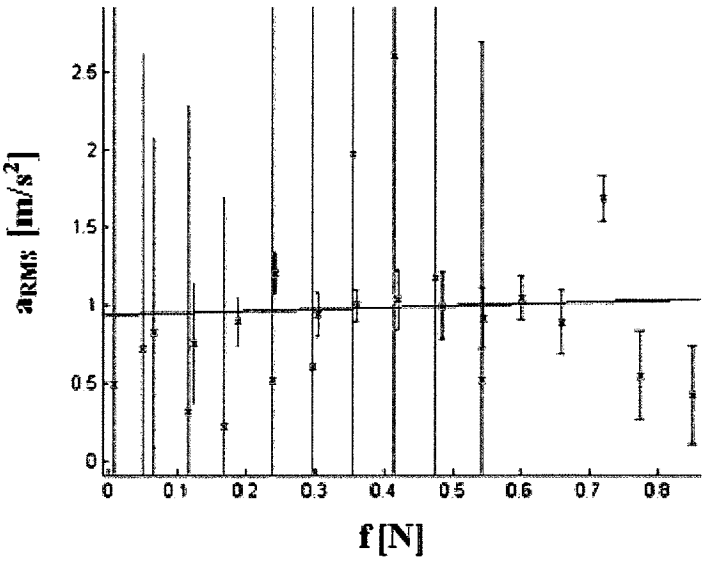

Figure 19: Linear approximation of the dependency of acceleration on force for Foam A with error bars.

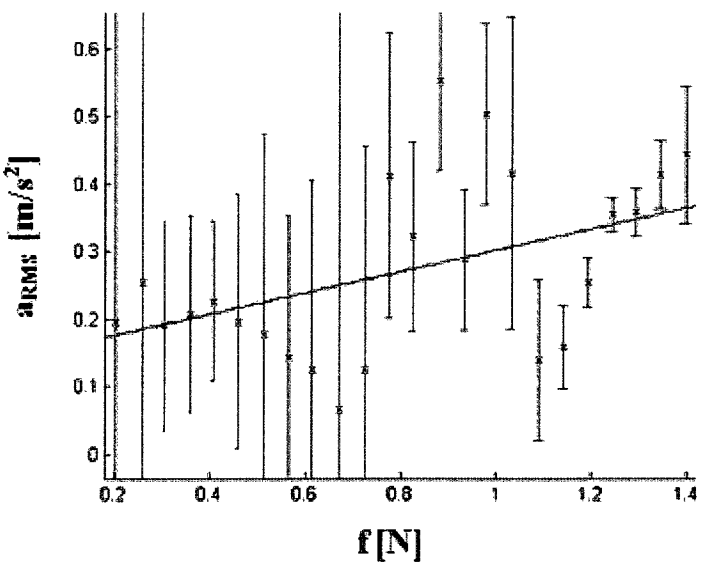

Figure 20: Linear approximation of the dependency of acceleration on force for Toy (foam) with error bars.

The Rubber tire is composed of uniform homogeneous structure with tightly packed molecules which allows scanning the surface with ease. In addition, the probe tip does

not get stuck while scanning due to rigidness of the Rubber tire. On the other hand, large variation in stiffness is observed in Foam A due to the composition of multi layered non-uniform cell structure. Compared to Rubber tire, it is far less rigid which make the scanning process uneven. The toy (foam) is more flat and homogeneous in outward appearance but with more complex internal cell structure with loosely packed cells. Scanning the toy (foam) with increasing amount of force does not vary the acceleration much. For some object materials like sandpaper, applying larger forces is not feasible due to its rough nature.

Thus the diverse characteristics of the materials such as arrangement of cells, molecules play an important role in determining the stiffness coefficients through the dynamic estimation method. In general, the advantage of this scanning procedure is it provides more number of samples and lets the user apply changeable forces. The values obtained from our scanning procedure support our argument by ranking the objects in terms of linear coefficient in the order of stiffness (hard to soft).

5.4 Summary

In this chapter we described compliance estimation methods for the contact stiffness of an object based on the acceleration and forces measured during stroking of its surface with WHaT. We conducted the experiments for multiple objects and estimate the compliance given by Lang and Andrew [LaAn09] by approximating a linear coefficient that relates force and acceleration results from multiple scans. In chapter 6, we show experimental results of the dynamic estimation compliance method and validated the model with a compression test results.

Chapter 6: Results

In this chapter we provide the results of our IIR filter based modelling of haptic vibration textures and estimation of compliance. Section 6.1 discuses output of the IIR filter model and validates the model by estimating the error between the original acceleration profile with respect to the IIR fitted model. Section 6.2 presents our compliance estimates for various stiffness objects. Section 6.3 throws light on haptic rendering of textures with our compliance estimate values.

6.1 Haptic Vibration Textures

We present results for three different types of profiles with three different scanning speeds for each. We choose the objects of different patterns. Sand paper follows a stochastic nature. Rubber mat consists of a repeating pattern and a jewel case contains regular ridges and grooves. Figure 21 portrays the scanning of the jewel case and the sandpaper. Figure 22, Figure 23 and Figure 24 shows the raw profiles for the jewel case, sandpaper and rubber mat under different scanning speed respectively. All the force-acceleration profiles are collected by stroking the real-world surfaces with the WHaT as described in chapter 3. The advantage of the system is to collect force-acceleration profiles from free-form surfaces i.e., our models can be estimated from surfaces measured on site. Otherwise, collecting data from physical environments can be quite tedious and may even prevent the use of reality-based models for virtual environments.

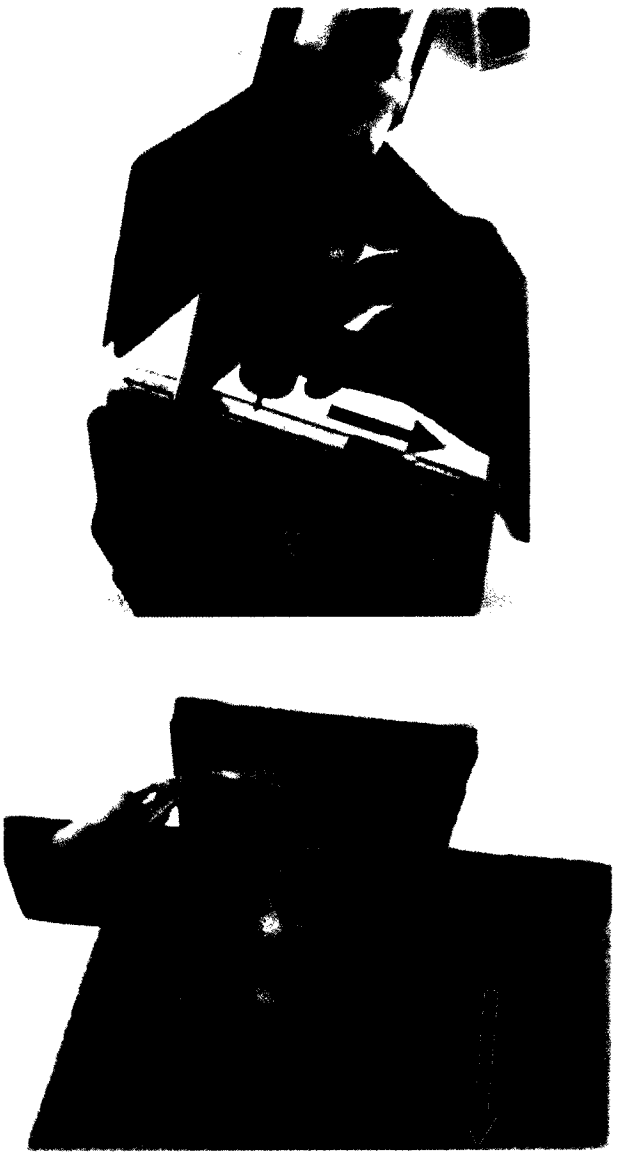

Figure 21: Scanning jewel case (top) and sandpaper (bottom) in the direction shown by arrow.

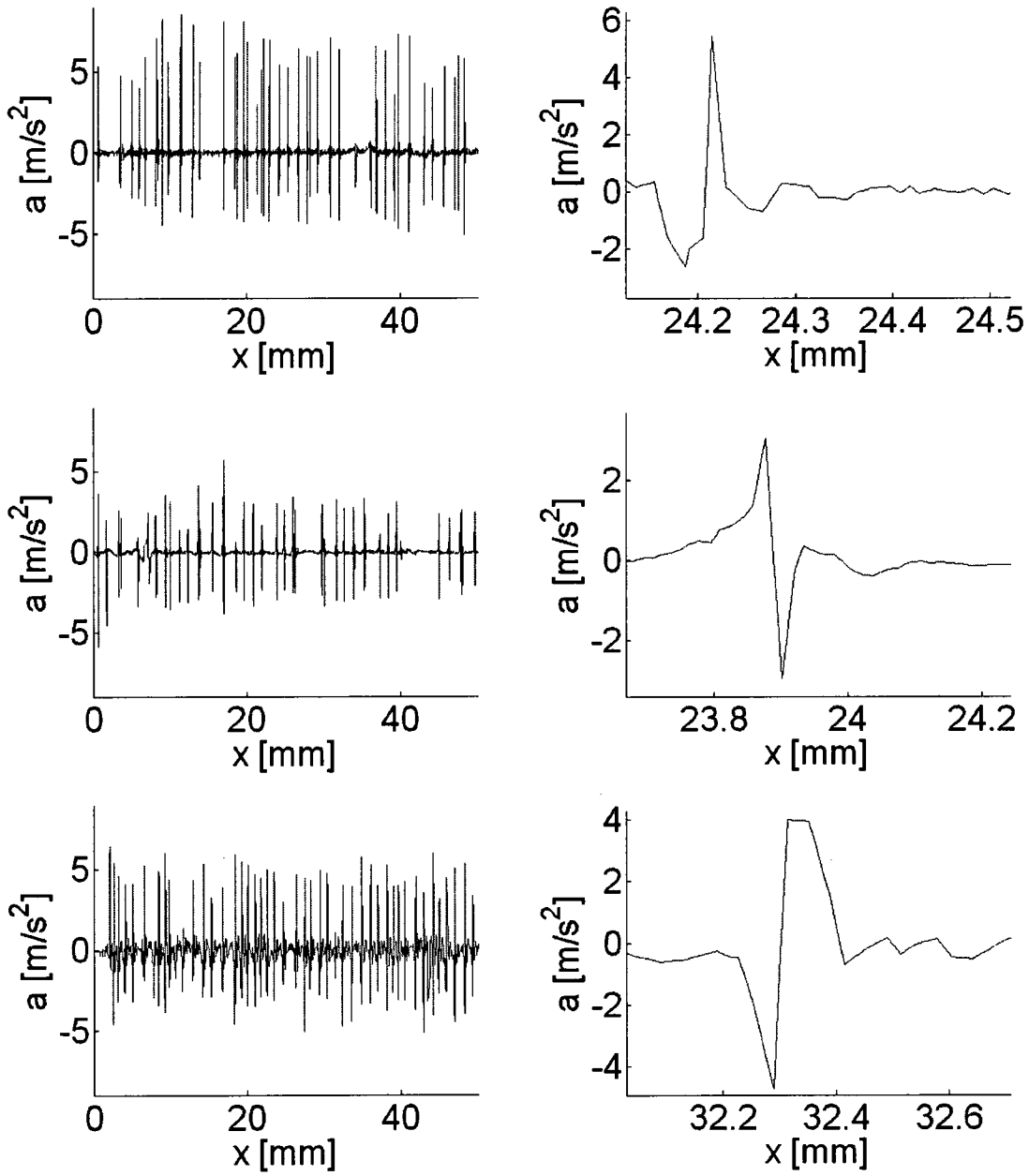

Figure 22: Left column shows raw acceleration profiles of jewel Case with different average scanning speeds. Top with 0.037m/s, middle with 0.044 m/s and bottom with 0.095 m/s respectively. Right column shows magnified view of single feature for corresponding speeds.

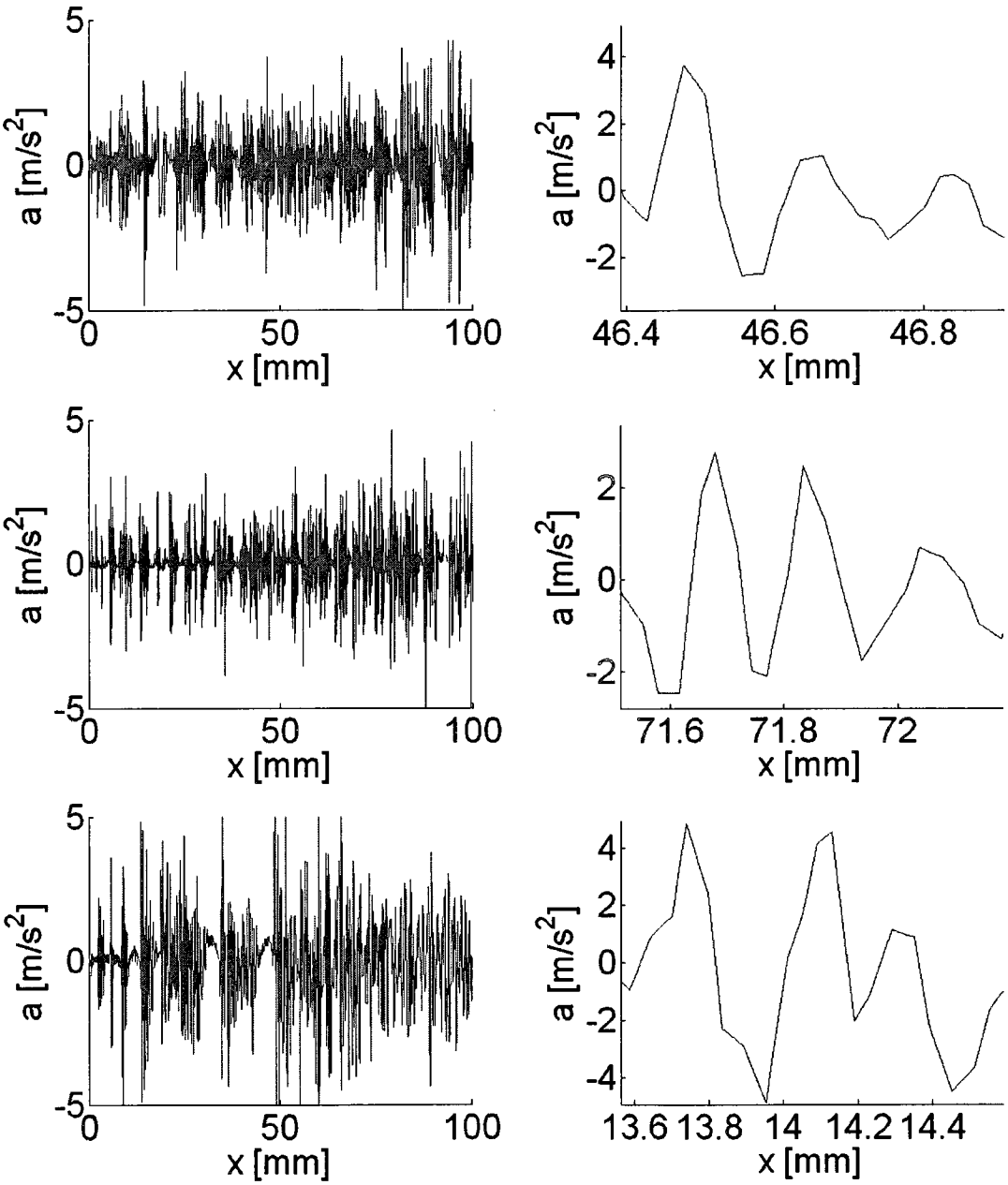

Figure 23: Left column shows raw acceleration profiles of sandpaper with different average scanning speeds. Top with 0.114m/s, middle with 0.123 m/s and bottom with 0.226 m/s respectively. Right column shows magnified view of single feature for corresponding speeds.

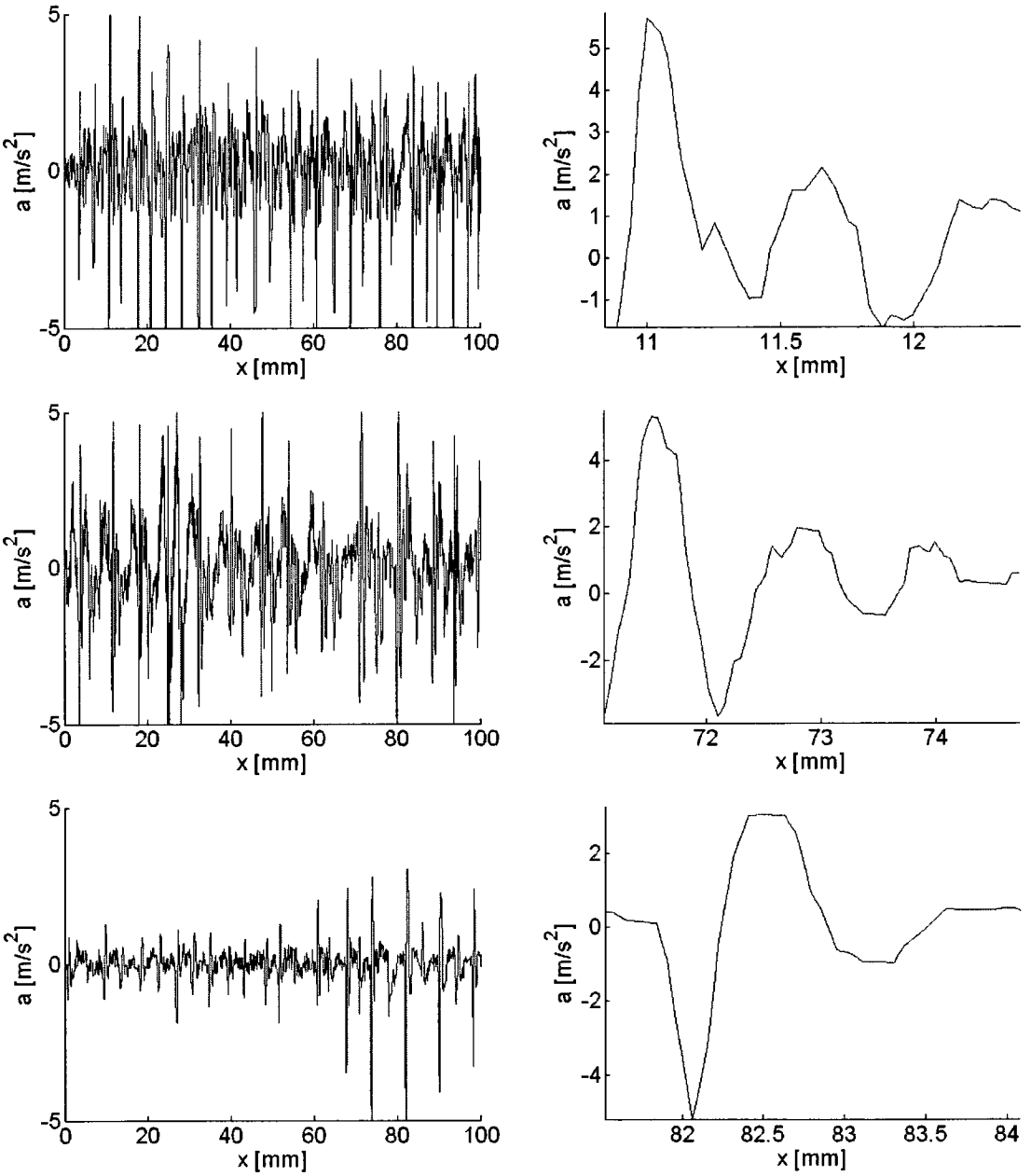

Figure 24: Left column shows raw acceleration profiles of rubber mat with different scanning speeds. Top with 0.135m/s, middle with 0.195 m/s and bottom with 0.222 m/s respectively. Right column shows magnified view of single feature for corresponding speeds.

We first apply a bandpass filter to the raw acceleration profile to ease the segmentation of the profile. The cut-off frequencies for the bandpass filter, f_{min} and f_{max}, is chosen by analyzing the frequency spectrum of the acceleration profile. The f_{min} and f_{max} is

located surrounding the dominant frequency in the frequency spectrum. The band pass filter is a 5th order Butterworth filter. We use Matlab's built-in function butter to implement the filter. We segment the acceleration profile in space to find the features and fit the acceleration profile in time as discussed in Section 4.3.2.

Table 1: Results for the estimation of the IIR filter model with cutoff frequencies of bandpass filter (f_{min} - f_{max}) fixed for three profiles.

Surface (f_{min} – f_{max})	*Avg. speed (m/sec)* (a)	f_{major} (b)	*Number Of Segment* (c)	*Total Length (mm)* (d)	$\frac{\#\ of\ Segments}{Total\ Length}$ (e)	$\bar{M}$+1 and $\bar{N}$+1 (f)	$\overline{SAD}$ in (m/s^2) (g)
jewel-case	0.037	0.122	1173	103.081	11.379	6.706	0.0028
(0 – 0.167)	0.044	0.018	542	72.836	7.441	7.444	0.0038
	0.095	0.063	251	53.556	4.686	6.993	0.0025
sandpaper	0.114	0.128	758	149.259	5.078	5.065	0.0008
(0.083 –	0.123	0.117	690	145.463	4.743	5.133	0.0006
0.151)	0.226	0.108	389	156.568	2.484	5.184	0.0009
rubber	0.135	0.023	206	125.676	1.639	7.192	0.0042
Mat	0.195	0.045	178	160.967	1.105	7.291	0.0043
(0 – 0.123)	0.222	0.048	171	166.388	1.027	7.009	0.0042

The IIR filters obtained with Prony's method have varying degree depending on the number of extrema per segment and the quality of fit. An error fit for our estimated IIR model through prony's series is also computed with respect to the bandpass filtered profile. We choose the filter which has minimum fit error with respect to the bandpass

filtered profile. Table 1 represents the estimated parameters for the three objects under three different scanning speeds **(a)** (c.f. Figure 22, Figure 23 and Figure 24). Please note that an average scanning speed is taken into account. "f_{major}" (**b**) represents the major frequency of the texture profile observed in the frequency spectrum. The "**Number of Segment**" **(c)** is the total number of segments estimated by our segmentation routine for the given scan length of the profile. The "**Total Length**" **(d)** gives the total scanned length of the corresponding profile for three different scanning speeds. The column **(e)** gives the average number of segments in a given $1mm$ scan length. "$\bar{M}$**+1 and** $\bar{N}$**+1**" **(f)** gives the average order of IIR filter estimated using prony's method and "$\overline{SAD}$ **in (m/s^2)**" **(g)** the error fit with respect to the bandpass filtered profile for the three profiles used. It should be noted that as the user is allowed to follow a free-path and can employ different scanning speed while scanning the surface, not all the features of the same profile are collated at the same position. The raw acceleration profiles presented in Figure 22 to Figure 24 are plotted on the equal axis for different scanning speeds and for different scanning length for comparison. The cutoff frequencies of band-pass filter, f_{min} and f_{max}, have been fixed for the different scans of each object. The cutoff frequencies are estimated from the frequency spectrum of the corresponding acceleration profile. It is estimated by surrounding the local minima of the major frequency obtained in the frequency spectrum. As the major frequency varies for different scans, we fixed the cut-off frequency for each profile irrespective of their scanning speed and dominant frequency. Figure 25 shows the frequency spectrum of the rubber mat.

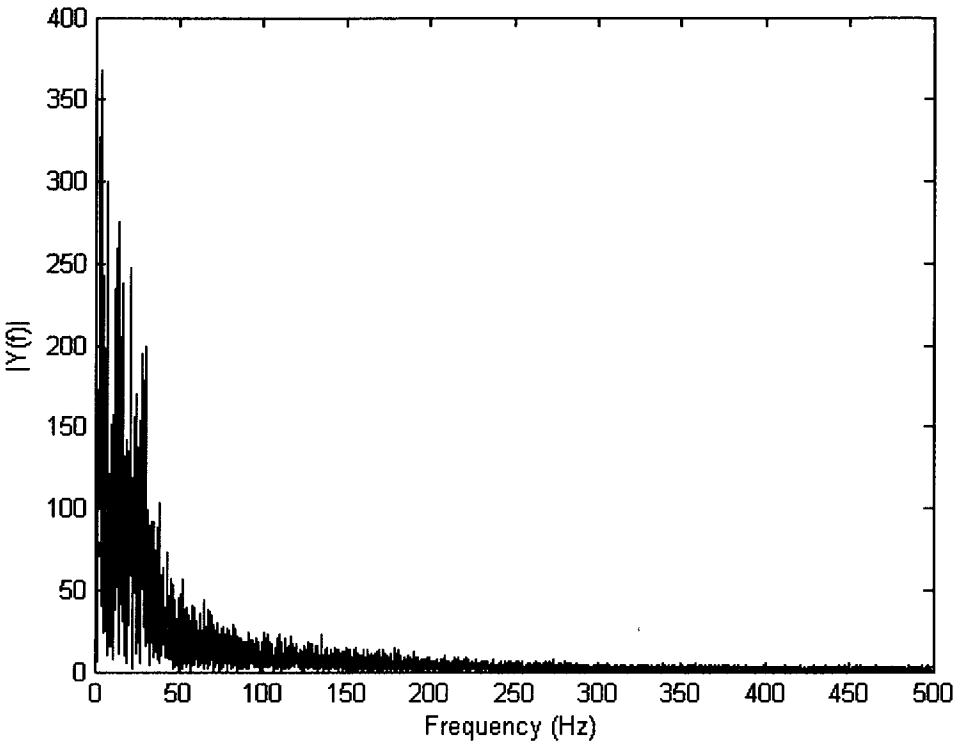

Figure 25: Frequency spectrum of the rubber mat

The fitted profiles through IIR filters for the three objects - jewel case, sandpaper and rubber mat are shown in Figure 26, Figure 27 and Figure 28 respectively. Our approach succeeds for all the three profiles independent of their characteristics.

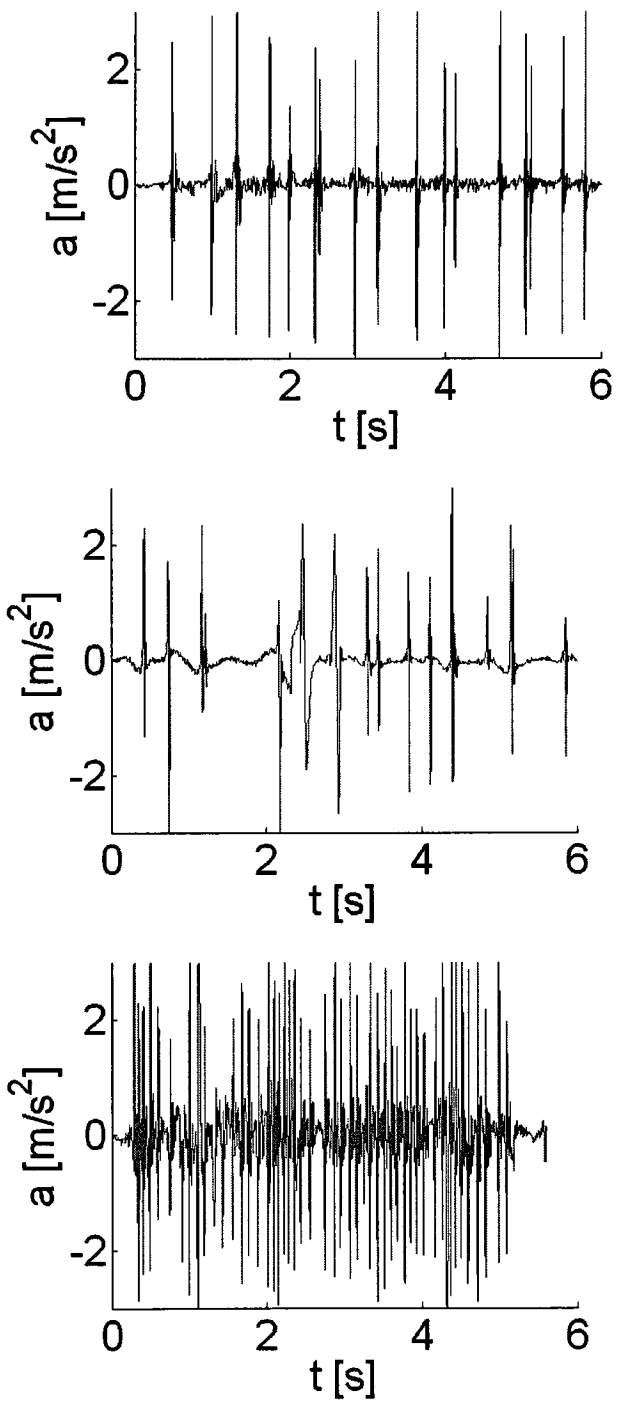

Figure 26: Prony Fit for the jewel case profile shown in Figure 22. Top with 0.037m/s, middle with 0.044 m/s and bottom with 0.095 m/s average scanning speeds respectively.

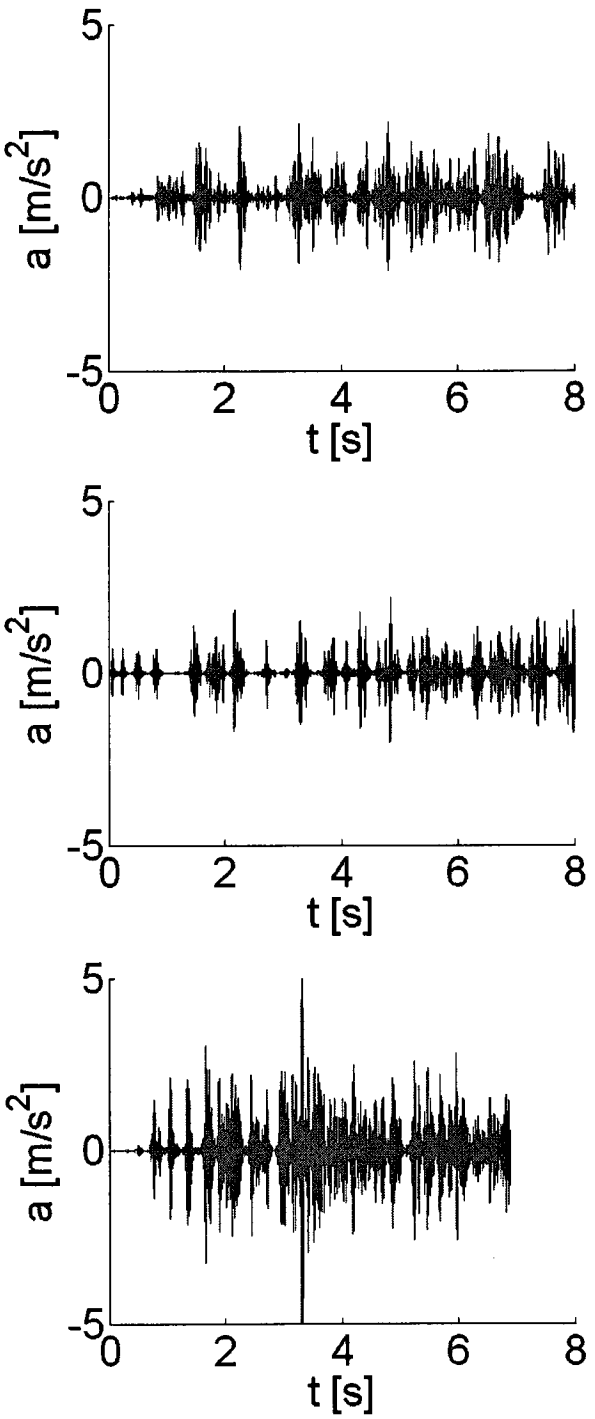

Figure 27: Prony Fit for the sandpaper profile shown in Figure 23. Top with 0.114m/s, middle with 0.123 m/s and bottom with 0.226 m/s average scanning speeds respectively

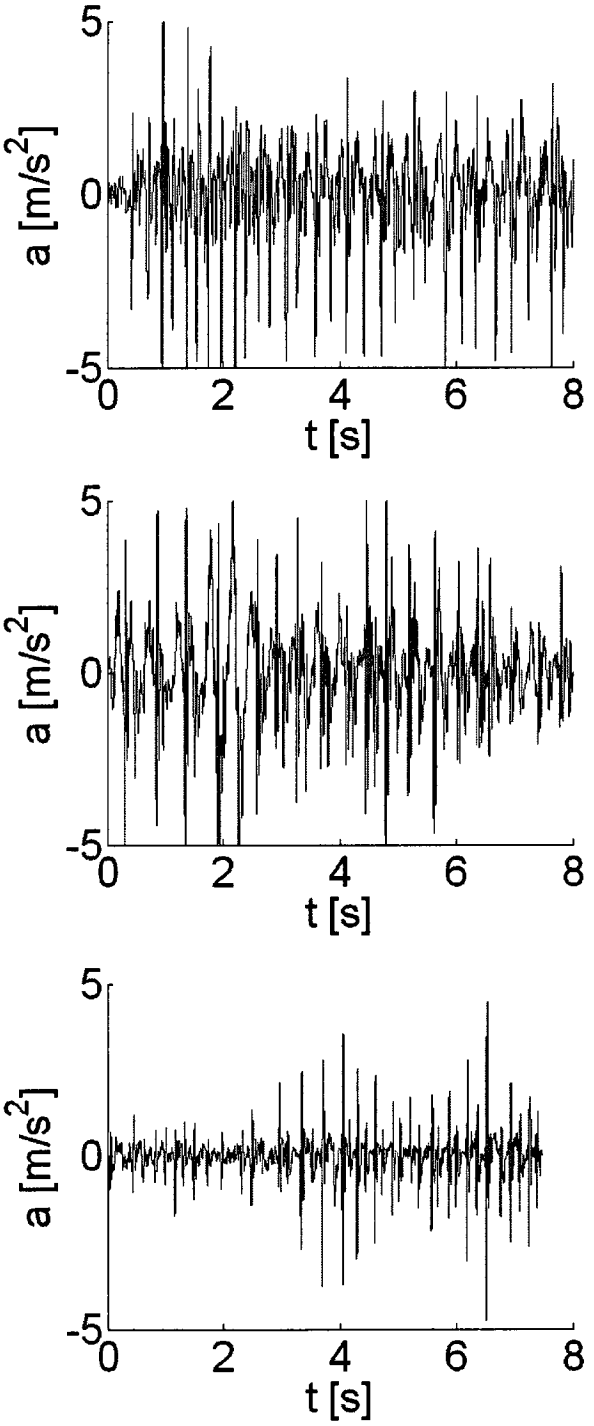

Figure 28: Prony Fit for the rubber mat for the profile shown in Figure 24. Top with 0.135m/s, middle with 0.195 m/s and bottom with 0.222 m/s average scanning speeds.

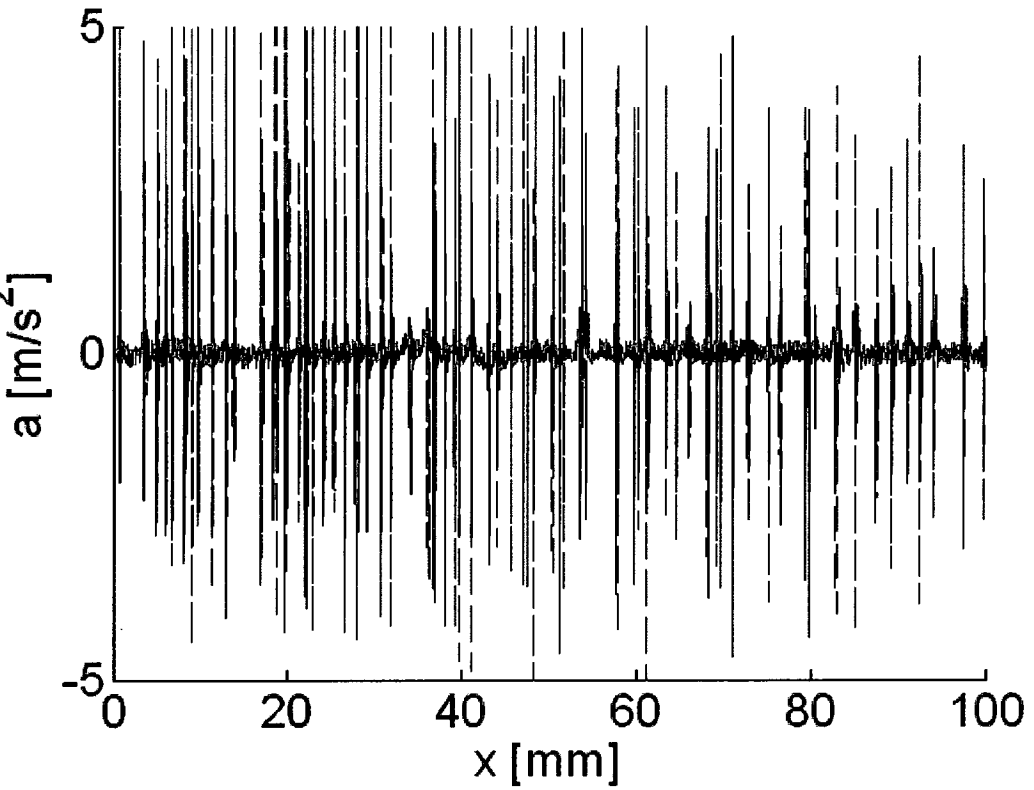

Figure 29: Comparison of IIR fit on the band-pass filtered acceleration profile. The green line shows the band-pass filtered acceleration profile and the black dashed line is the IIR fit

In general, while the amplitude of our acceleration profile varies in accordance with the force the user scans, no significant variance is observed on the velocity with which user scans. We do not take into account Okamura et al.'s claim that the amplitude also depends on the scanning velocity. We also observe that even as the user scans the surface at any speed, the characteristic frequencies of the features remain constant but the damping is more dependent on the nature of the material than the velocity. With a higher speed, more number of features are covered per unit length. We analyze the data from Table 1 to see which parameters have more influence over variations in scanning speed.

- For sandpaper, the major frequency remains stable with variation in scanning speed. This shows that scanning velocity is independent of characteristic frequency of the profile. However, the number of segments per unit length doubles with an approximately twofold increase in scanning speed. Even though the sandpaper has an inherent stochastic nature, a methodological relation is observed with respect to the scanning speed. Among the three objects, the major frequency of sandpaper is the highest. This could be due to the stochastic nature of sandpaper.

- For rubber mat, we observe a proportional increase in the major frequency with the increase in scanning speed. We assume that this variation is due to the dominance of spatial frequency over the characteristic frequency of the profile. Rubber mat contains regularly arranged ridges and grooves. These spatially located features contribute to the major frequency unlike sandpaper, where a stochastic characteristic nature is predominant. The major frequency of rubber mat is lowest compared to other two objects.

- For jewel case, it does not show any significant variations in correlation with the scanning speed. The major frequency shows an unstable nature and could not be predicted with the varying scanning speed. However, from the analysis of error fit value for all of the three profiles, our IIR estimation method fits the profile approximately. We plot our IIR filter profile on top of the band-filtered acceleration profile to show visually how our model fits the profile. Figure 29 shows the overlap of estimated IIR model on bandpass filtered signal for jewel case.

6.2 Compliance

In this section, we present the compliance values estimated of various objects ranging from hard materials such as sandpaper to soft materials like mouse-pad through the line fitting process. The compliance estimates $\tilde{\kappa}_c$ are validated against a compression test that truly measures the deformation of the object by applying forces. The compression test set-up is shown in Figure 30.

Figure 30: Compression test: The probe augmented to the 6D force-torque haptic device. The user measures the applied force and the displacement undergone by the object

The compression test is carried out by connecting a 6D force-torque sensor (ATI Nano 25) with a spherical indenter of radius R=0.265 mm to the haptic device (MPB Freedom 6S). The user applies required compressional force to deform the object within the elastic

limit and the stress experienced by the object is recorded. Figure 31 shows the plot of force and displacement values measured for the cork. The compression test is repeated number of times to accommodate the dynamic nature of the user applied force.

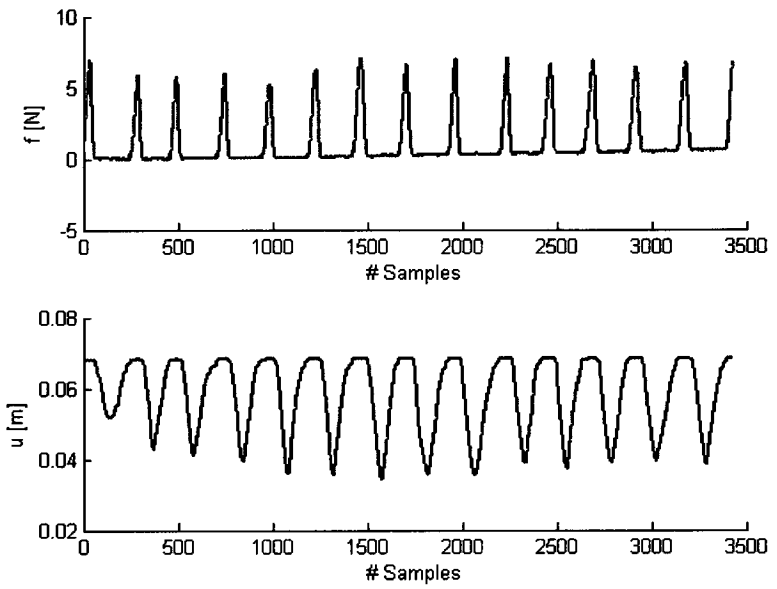

Figure 31: Force and displacement

Since most of our objects are of ductile nature, we consider an elastic deformation and fit a Hertzian sphere-plane contact model to the measurements given by

$$f = \frac{4}{3}\sqrt{R}\frac{E}{1-\sigma^2}u^{\frac{3}{2}} = \frac{4}{3}\sqrt{R}E_r u^{\frac{3}{2}} = \tilde{k}_{comp}u^{\frac{3}{2}}$$

where E and E_r are the Young's modulus and the reduced Young's modulus, and σ is the Poisson's ratio of the object. By substituting the values into the equation, we calculate the stiffness of the material $\tilde{k}_{comp}$. We first segment the curves into individual compression curves as shown Figure 32 and fit a Hertzian contact model to each segmented curve separately. Figure 33 shows the fit for one linear curve. First the data from the recordings

is partitioned into individual compressional curve and then a Hertzian contact model is applied to each curve. Figure 32 shows the data and Figure 33 shows the Hertzian fit

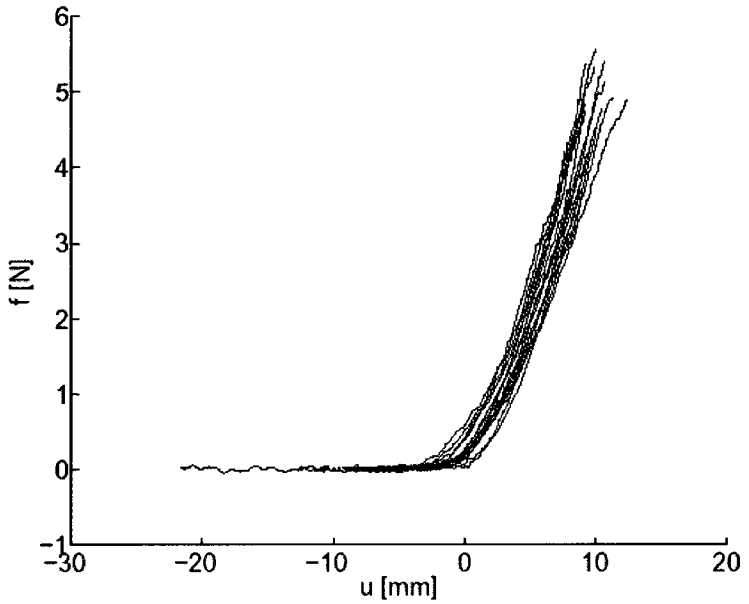

Figure 32: Data recorded from Freedom 6S Device

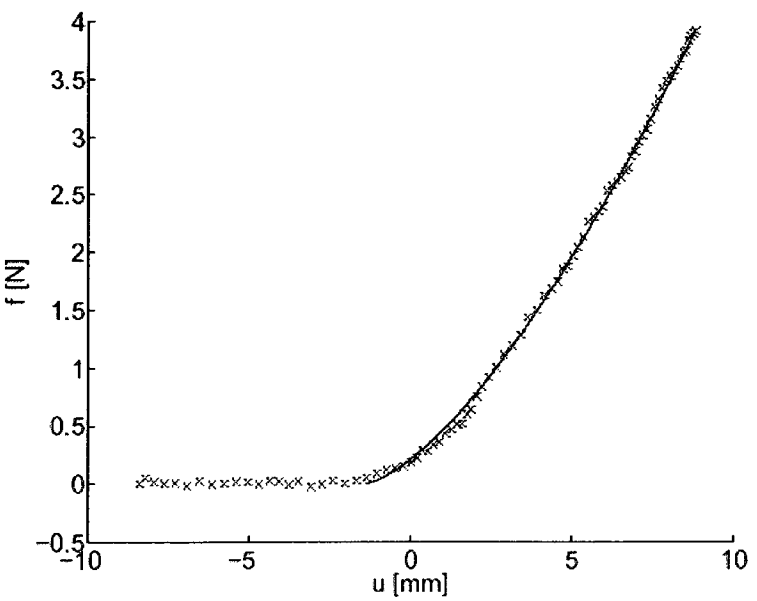

Figure 33: Hertzian contact fit

The Table 2 lists the compression coefficients, $\tilde{k}_{comp}$, reduced young's modulus, $E_r[MPa]$, from the compressional test and the compliance coefficient k_c with standard deviation of fit, σ, for all the objects. The compliance estimation method successfully ranked the object according to the stiffness coefficients from compression test. The images of the corresponding objects with the scanning direction are shown in Appendix. Please note that the images Sponge B (also referred as rubber mat) and sandpaper is shown in Figure 2 and in the lower image of Figure 21 respectively.

Table 2: Experimental verification from a spherical indentation test. Stiffness estimates (k_c) and standard deviation of fit (σ) for several materials are found using the compliance estimation using WHaT device. The other two parameters are obtained from the spherical indentation device

Material	k_{comp}	E_r[MPa]	k_c	σ
Sandpaper	n/a	n/a	0.907	0.725
Cork	49	14.7	0.853	0.257
Rubber tire	39.4	11.8	0.526	0.096
Toy (crocodile)	25.8	7.74	0.266	0.145
Pencil eraser	13.2	3.97	0.179	0.112
Floor felt	9.14	2.74	0.163	0.038
Toy (foam)	4.02	1.21	0.157	0.102
Sponge A	3.29	0.986	0.132	0.054
Sponge B	1.56	0.469	0.117	0.055
Foam A	1.83	0.548	0.115	0.31
Mouse pad	0.276	0.083	0.108	0.02
Foam B	0.212	0.063	0.108	0.059

The compression test values by this 6D force-torque haptic device are used solely to evaluate stiffness estimation method using WHaT device. Additionally, an empirical relationship between the reduced young's modulus, $E_r[MPa]$, and the compliance coefficient k_c is estimated and an exponential curve is fitted with the aid of matlab's fminsearch routine. The relationship is given by

$$k_c = 0.0217 + 0.0883e^{0.149E_r[\frac{1}{MPa}]}$$

Figure 34 shows the corresponding relationship of the above equation.

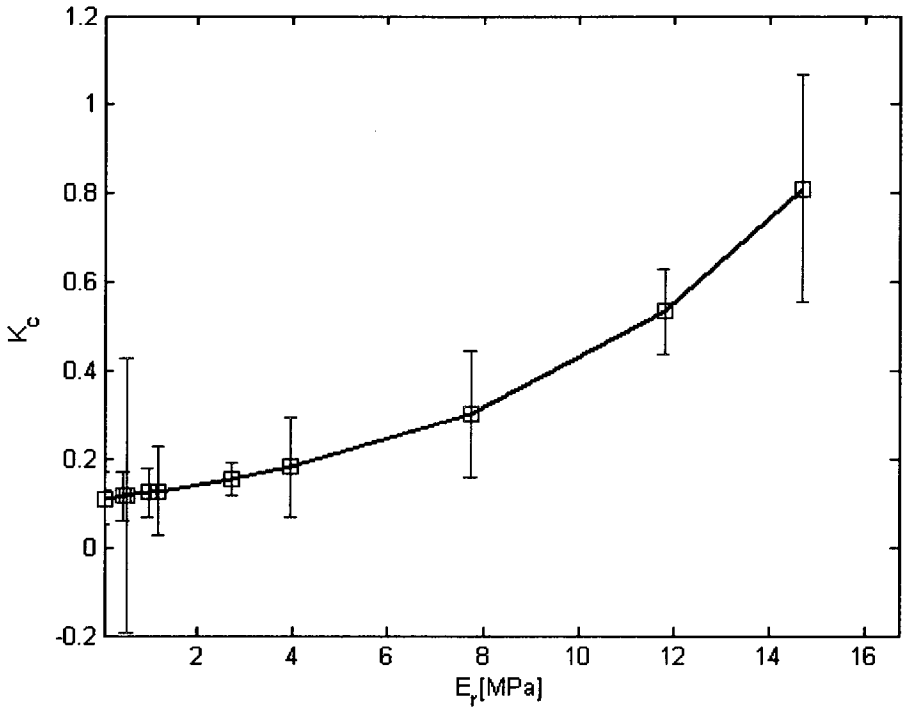

Figure 34: Relationship between E_r and compliance estimate k_c

The point to be noted here is that the stiffness estimation method for k_c from our scans assumes that the object's surface is not smooth, i.e., the surface contains some features, since we require accelerations normal to the average surface. The object must also be reasonably homogeneous. For example, as discussed in Section 5.3, the estimate for packaging foam A is likely due to the foam having large variations in stiffness due to an internal coarse cell structure. The scanning procedure signals this issue with a high fitting error.

6.3 Haptic Rendering

For haptic rendering of our texture, we adapt the model of Andrews as discussed in chapter 3 of his thesis [Andr07] in which the haptic interaction point on the triangulated object surface is parameterized as a position along the 1D profile and a distance normal to the profile. The mapping is performed with the help of barycentric coordinates. But differently from the method of rendering a height profile in [Andr07] we directly use the acceleration profile. Our haptic rendering employs a penalty-based approach where the penalty force is composed of a rigid body constraint force plus a texture force normal to the surface plus a lateral frictional force.

The following equation shows the resultant force f_{result} as the summation of normal surface constraint force, f_c, texture force, f_t f_t and friction force, f_f f_f [SiPa96].

$$f_{result} = f_c + f_t + f_f$$

We change the normal texture force to the scaled acceleration profile as produced by the IIR filter. The normal texture force is the sum of all K currently active filters. A filter becomes active once the haptic interaction point has traversed the filter location x_k on the profile at discrete sampling time, $-t_k = -cT$. The overall normal texture force is then given by

$$F_t(z) = \sum_{k=0}^{K} A_k z^{-t_k/T} H_k(z)$$

where

$$H_k(z) = \frac{\sum_{i=0}^{M_k} b_{ik} z^{-i}}{\sum_{j=0}^{N_k} a_{jk} z^{-j}}$$

with $N_k \geq M_k$ and $a_{0k} = 1$ for all filters.

We use the compliance estimates from our dynamic estimation method in our haptic rendering of textures. The stiffness coefficients are used to modify the stiffness of textures when they are displayed to users through a haptic interface in a hapto-visual application. When using a very rigid stiffness value, such as the sandpaper, we consider that the textures are pronounced and salient texture features are easily detectable. For lower stiffness values, texture features are attenuated, with the soft mouse-pad being mostly characterized by rigid body contact forces. We currently render our texture with a stylus-based haptic device (for example PHANTOM desktop) with a haptic update rate close to 1 kHz.

6.4 Summary

This chapter illustrated the results of our reality-based approach to model the vibrotactile textures and estimate the compliance. Here, we simulated vibrotactile texture for different objects ranging from stochastic to regular patterned textures. We used our dynamic compliance estimation method to find the compliance coefficient for a set of specimens with different stiffness ranging from a soft mouse pad to sand paper. Our compliance estimation method successfully ranked the objects according to stiffness from the compression test. We also described haptic rendering using the texture force obtained from scanning an object.

Chapter 7: Conclusion and Future Work

7.1 Summary

This chapter provides a summary of the research work presented in this thesis. The core of this thesis is devoted to developing a novel and adaptable method to acquire and represent two significant dimensions of haptic perceptions - texture and compliance.

7.1.1 Vibrotactile feedback Textures

We developed a novel method to obtain vibrotactile haptic textures from real-world samples. Our novel texture model consists of spatially distributed and computationally efficient IIR filters which operate in the time-domain. With the help of IIR filter design through Prony's series, we could replicate the vibrations that are obtained while scanning the real-world surface textures. Our modeled vibrations that are matched with the real world data enhance the virtual environment by making it feel more physical. During rending of the profiles, the textured surface can be traversed at any speed and the spatial frequencies of the features remain constant but the damping is dependent on the velocity. Our procedure extends and unifies the decaying sinusoid approach which has been proposed by others previously. Our estimation method is able to estimate suitable IIR filters for stochastic, patterned and mixed surfaces. The method is based on segmentation and the use of Prony's method for IIR filter design.

A flaw of our model is time-aliasing which is encountered during scanning. Time aliasing occurs if the decaying wave of one feature has not significantly diminished before the next feature is encountered. Our current approach to the above issue is to simply truncate the earlier decaying wave and start a newly generated vibration waveform at each feature with the complete signal. This is not visible if the user's speed during scanning and rendering are well matched, but may lead to potential errors, especially, if the motions during rendering are slower than the ones during scanning.

7.1.2 Compliance

We also conducted experiments to present the statistical approach of estimating the stiffness coefficient for haptic texturing. The method estimates the coefficients solely based on the analysis of the force and acceleration during a surface scan and we are able to show an experimental relationship to the contact stiffness as measured during the compression. We provide the compliance coefficients for a broad range of object ranging from a soft mouse-pad to sandpaper. The compression test is carried out for all the objects except sandpaper for independent verification of our dynamic stiffness estimation method based on scan profiles.

One of the requirements of compliance estimation method is that the specimens under test should not be smooth enough such that the resultant acceleration from scanning the surface is negligible. Another assumption we have made is that the specimens should have homogeneous structure.

7.2 Future Work

One of our future goals in vibrotactile texture modelling is to address different contact methods that occur in real-world scanning of textures. In the future, we would like to employ perceptual test to verify the effectiveness of vibration feedback models in haptic texturing. While doing so, we may need to scale vibration waveforms and choose scaling parameters that affectively render the vibration waveforms. The compliance estimation is based on statistical analysis of linear relation between force and acceleration. However, user studies can be performed to analyze the perception of compliance estimates. A series of experiments could be conducted to determine whether the users are able to distinguish between objects by using our estimated compliance coefficients. We also would like to improve the performance of our model by investigating the complexity of it.

Appendix

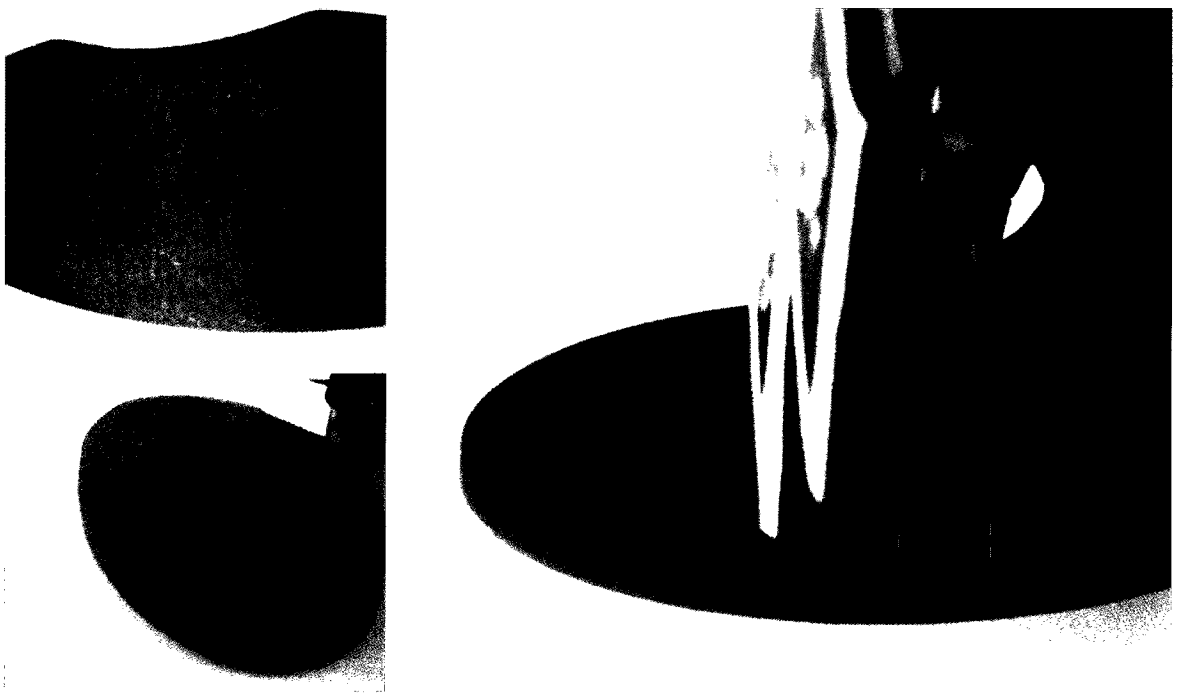

Figure 35: Scanning of mousepad in the direction shown by arrow

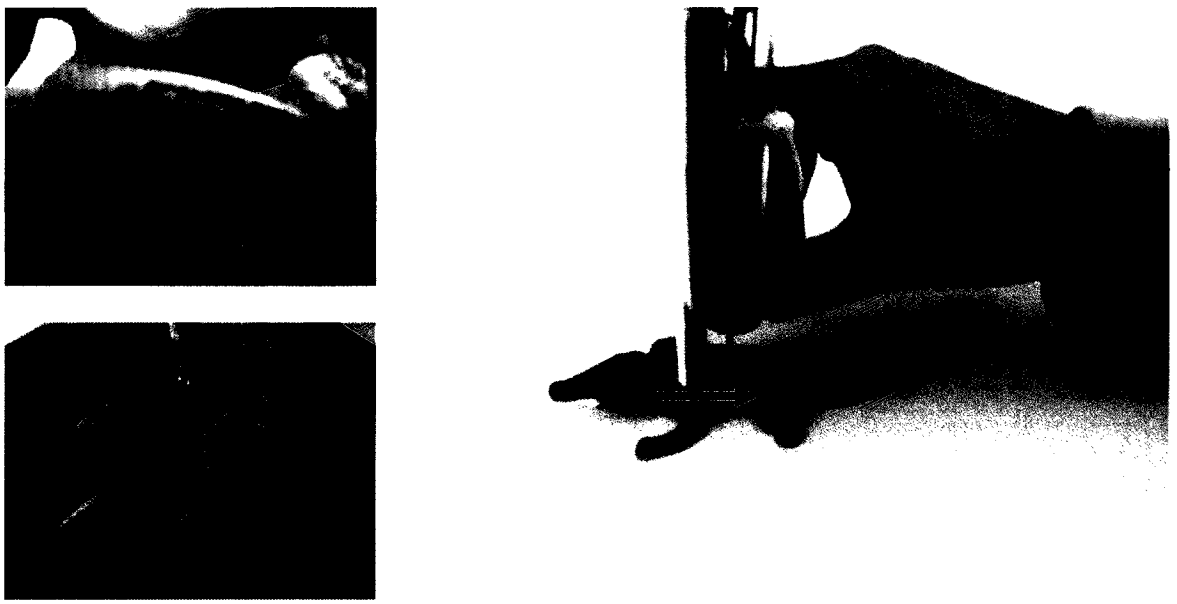

Figure 36: Scanning of toy (crocodile) in the direction by arrow

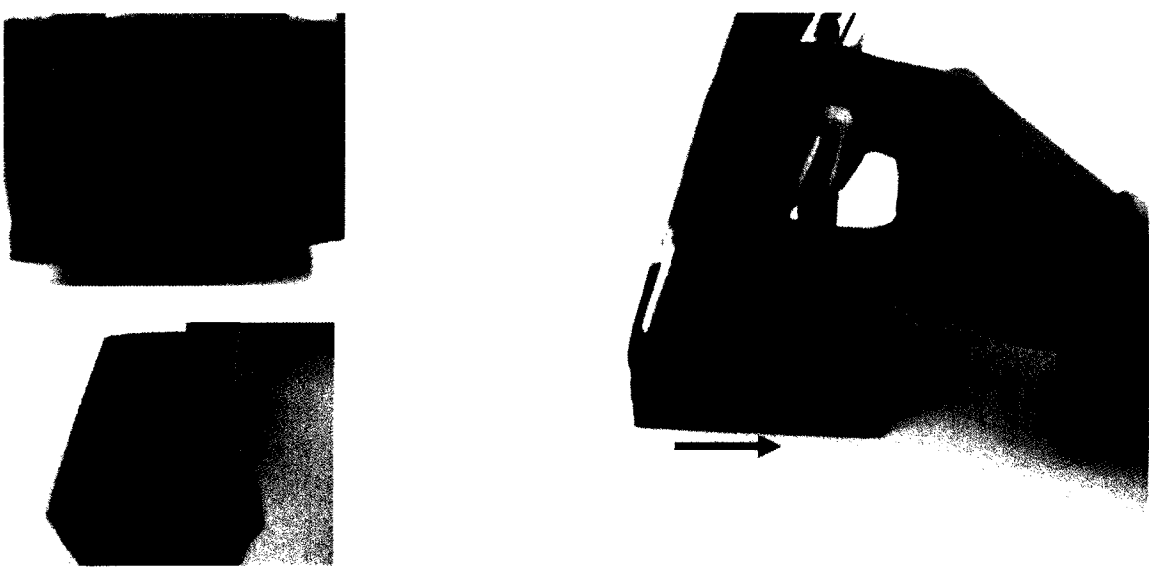

Figure 37: Scanning of Foam A in the direction shown by arrow

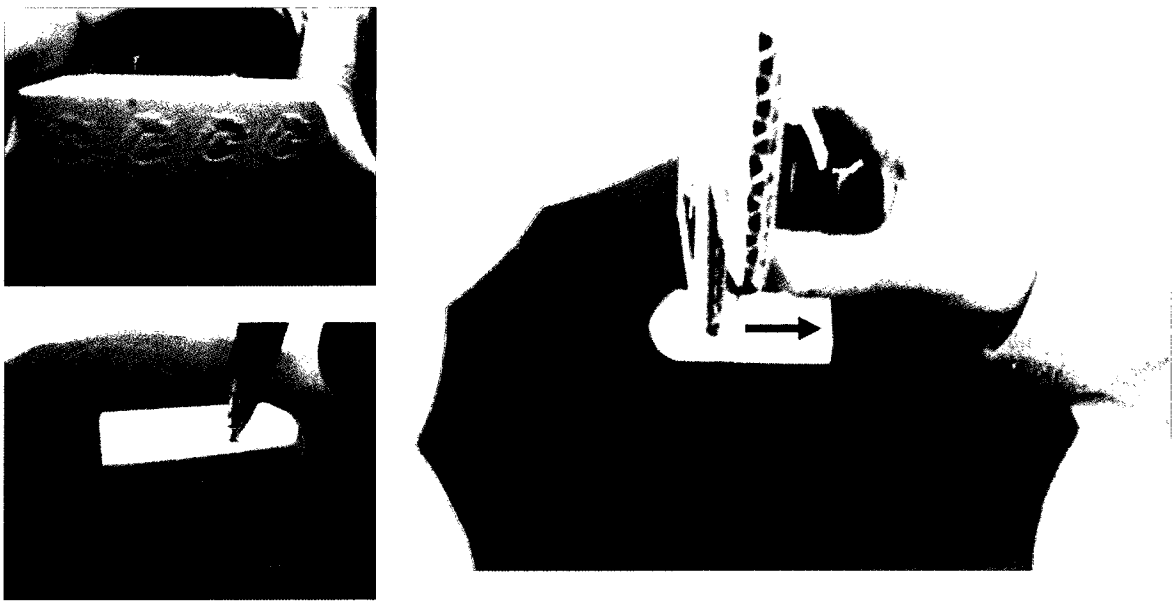

Figure 38: Scanning of pencil eraser in the direction shown by arrow

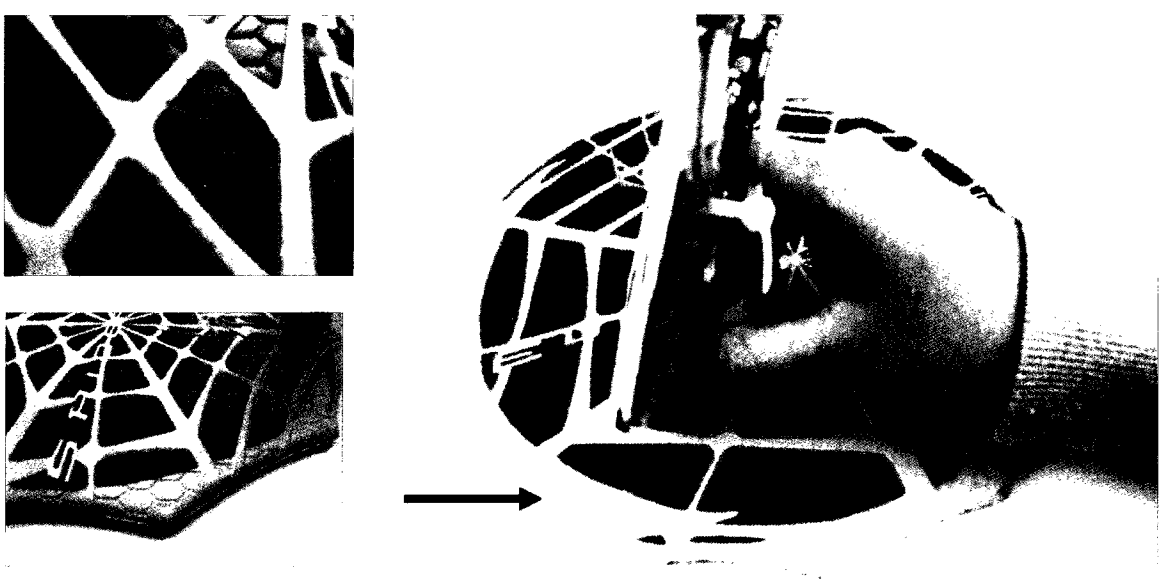

Figure 39: Scanning of patterned part of toy (foam) in the direction shown by arrow

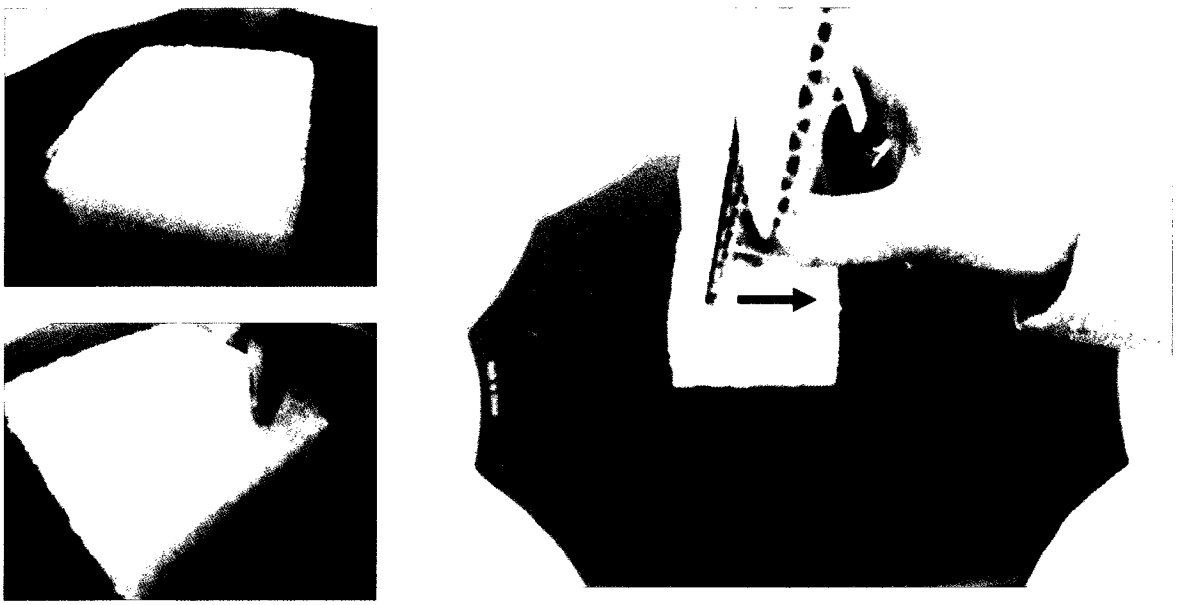

Figure 40: Scanning of Foam B in the direction shown by arrow

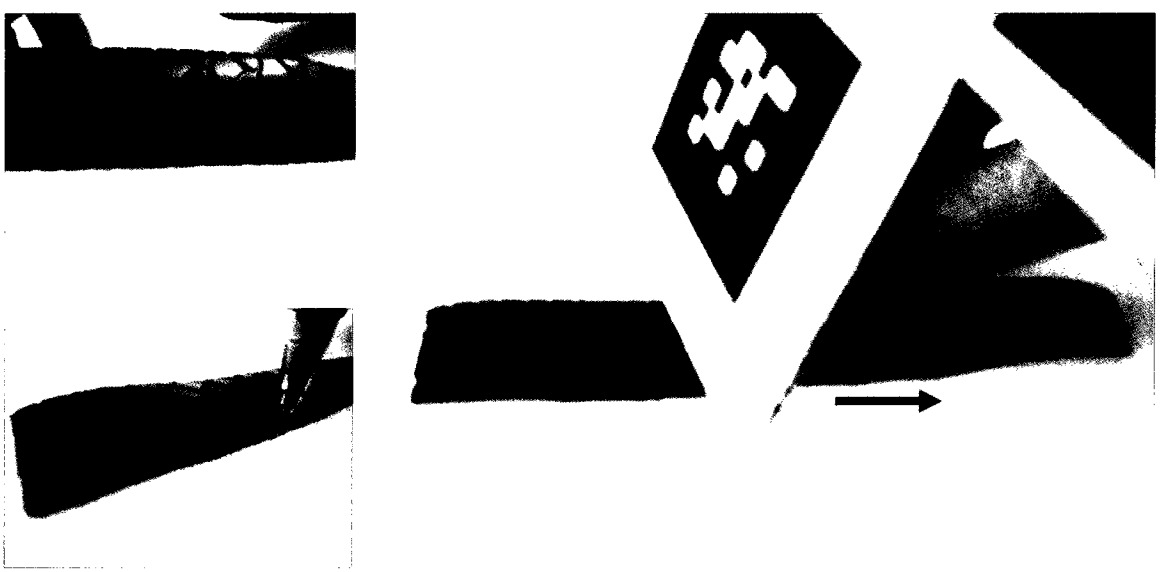

Figure 41: Scanning of rubber tire in the direction shown by arrow

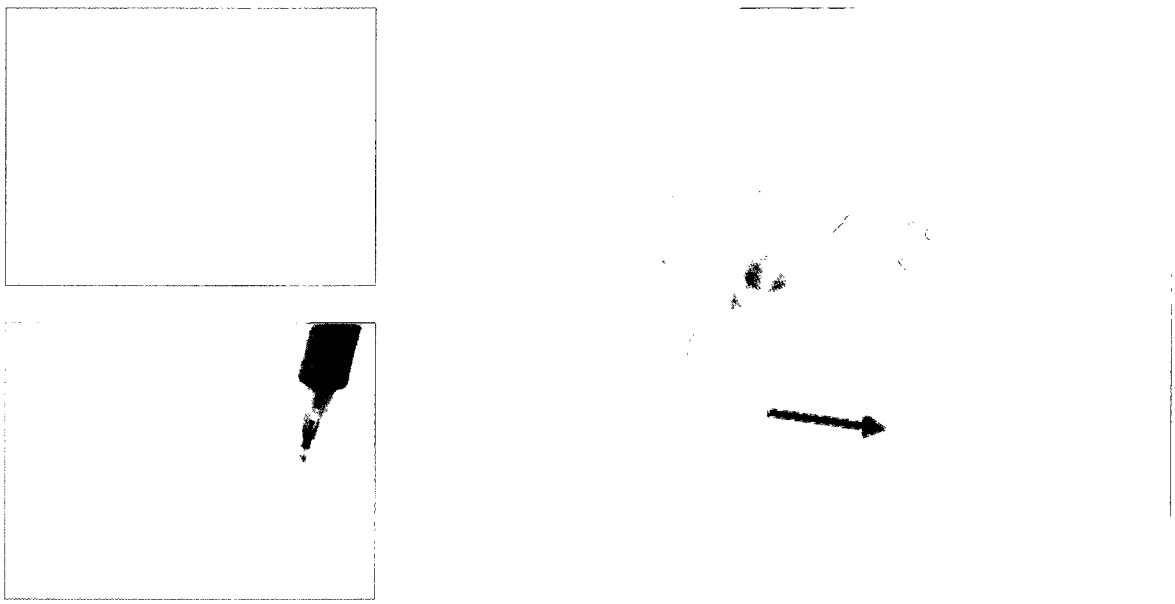

Figure 42: Scanning of floor felt (matted fabric) in the direction shown by arrow

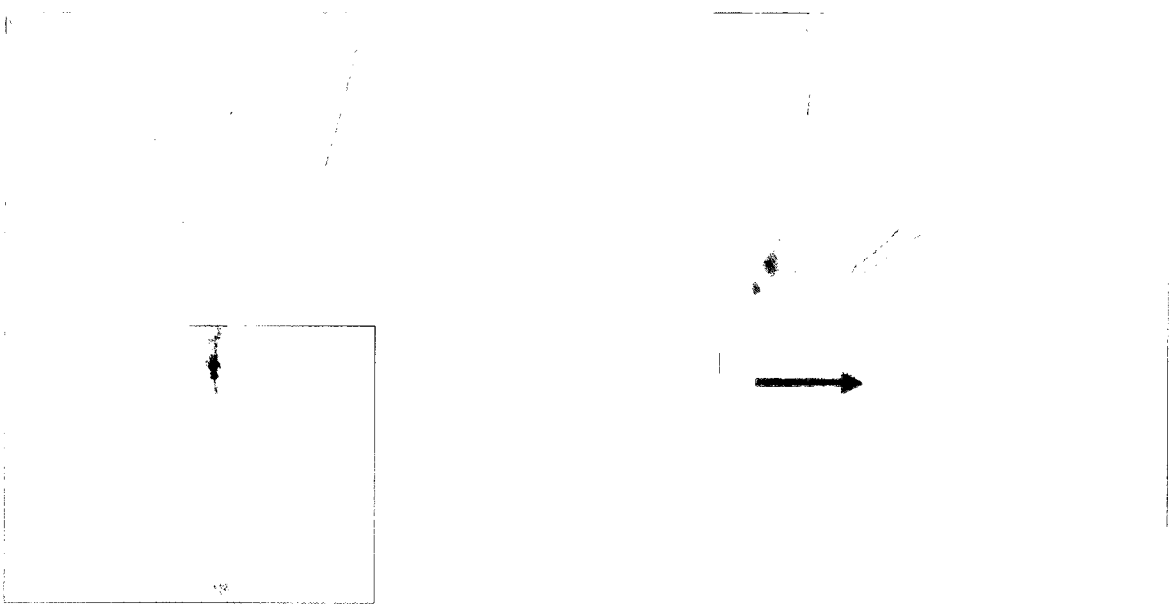

Figure 43: Scanning of cork in the direction shown by arrow

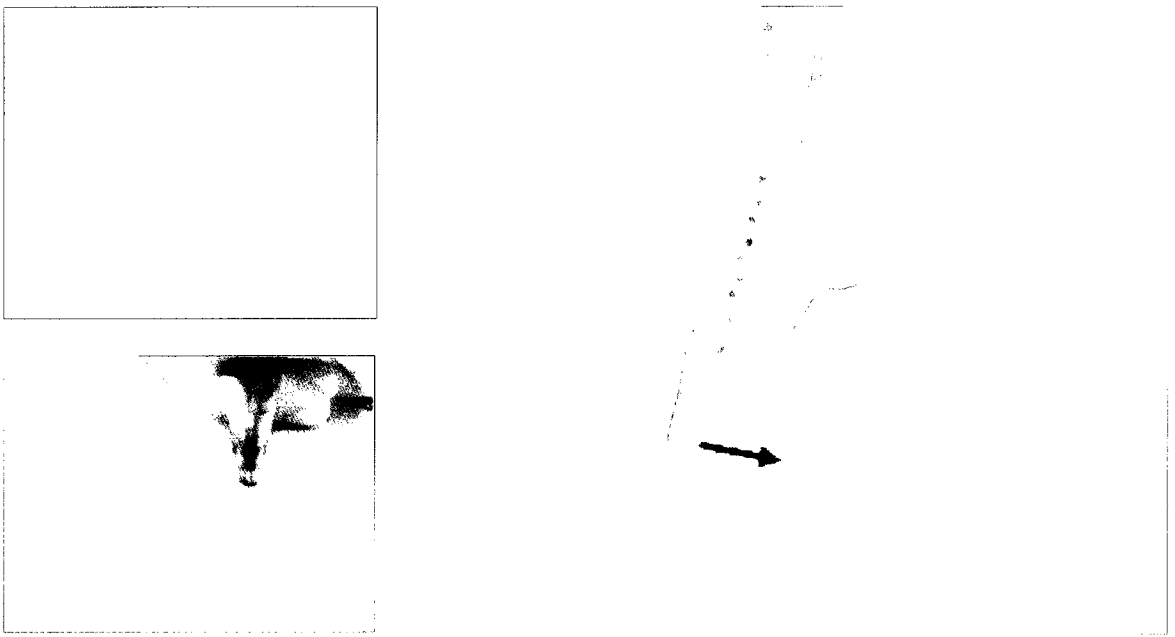

Figure 44: Scanning of sponge A in the direction shown by arrow

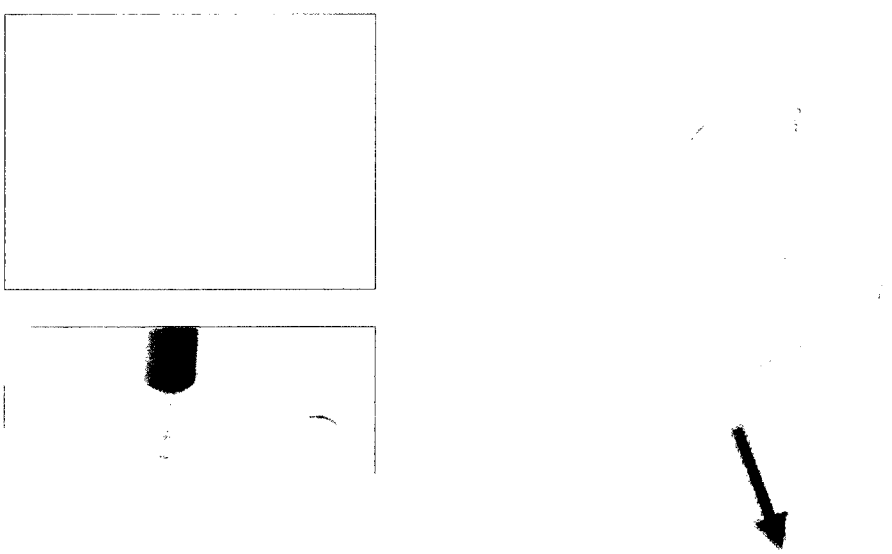

Figure 45: Scanning of rubber mat in the direction shown by arrow

Figure 46: Scanning of jewel case in the direction shown by arrow

References

[Andr07] Andrews S.: Measurement-based Modeling of Contact Forces and Textures for Haptic Rendering. Master's thesis, University of Ottawa, 2007

[AnLa07] Andrews S., Lang J.: Interactive Scanning of Haptic Textures and Surface Compliance. *Proceedings of 6th International Conference on 3-D Digital Imaging and Modeling (3DIM07), IEEE.*, pp. 99-106, 2007

[BRPG05] Ballesteros S., Reales J.M., Ponce de Leon L., Garcia B.: The perception of ecological textures by touch: Does the perceptual space change under bimodal visual and haptic exploration. *Proceedings of World Haptics Pisa. IEEE computer society.*, Los Alamitos, CA, 635-638, 2005

[BaHe08] Ballesteros S., Heller M.A.: Haptic Object Identification. *In Grunwald M (Ed.), "Human Haptic Perception".*, Birkhauser Verlag, pp. 207-222, 2008.

[BaCS97] Basdogan C., Ho C-H., Srinivasan M.A.: A Ray-based Haptic Rendering Technique for Displaying Shape and Texture of 3D Objects in Virtual Environments. *Proceedings of the ASME Dynamic Systems and Control Division.*, 1997

[BiSL86] Bier E.A., Sloan K.R.: Two part texture mapping. *IEEE computer graphics and applications.*, 40-53, 1986

[Blin78] J. F. Blinn.: Simulation of wrinkled surfaces. *In Proceedings of SIGGRAPH Computer Graphics* ., 12(3), pp. 286-292, 1978

[CBOZ04] Chi T., Ballinger T., Olds R., Zecchino M.: Surface Texture Analysis Using Dektak Stylus Profilers. Veeco Instruments Inc, 2004

[CoHo07] Colton M.B., Hollerbach J.M.: Reality-Based Haptic Force Models of Buttons and Switches Export. *In Robotics and Automation, 2007 IEEE International Conference on.*, pp. 497-502, 2007

[CuZR05] Cuevas E., Zaldivar D., Rojas R.: Kalman filter for vision tracking. Tech. Rep., Freie Universitat Berlin, 2005

[Fial04] Fiala M.: ARTag Revision 1, a fiducial marker system using digital techniques. *In NRC/ERB1117 Technical Report. National Research Council of Canada.,* 2004

[FrBa96] Fritz J., Barner K.: Stochastic models for haptic texture. In SPIE Intl. Symposium on Intelligent Systems and Advanced Manufacturing - Telemanipulator and Telepresence Technologies., 1996

[GOMG*06] Galoppo, N., Otaduy, M. A., Mecklenburg, P., Gross, M., and Lin, M. C.: Fast simulation of deformable models in contact using dynamic deformation textures. *Proceedings of the 2006 ACM Siggraph/Eurographics Symposium on Computer Animation.* Aire-la-Ville, Switzerland, pp 73-82. September 02 - 04, 2006

[HACG*04] Hayward V., Astley O.R., Cruz-Hernandez M., Grant D., Robles-De-La-Torre G.: Haptic Interfaces and devices. Sensor Review Emerald 24(1),pp:16-29, 2004

[HaCr00] Hayward V., Cruz-Hernandez M.: Tactile Display Device Using Distributed Lateral Skin Stretch. *Proceeding of the Haptic Interfaces for Virtual Environment and Teleoperator Systems Symposium, ASME IMECE2000.*, Vol. DSC-69(2), pp. 1309-1314, 2000.

[HaMa07] Hayward V., Maclean K.: Do it yourself haptics: part I. *IEEE Robotics & Automation Magazine.*, 14(4), pp. 88–104, 2007.S

[Harr09] Harris W.: How Haptic Technology Works. http://electronics.howstuffworks.com/gadgets/other-gadgets/haptic-technology.htm, Access Date: 2009-09-10

[Hell89] Heller M.A.: Texture perception in sighted and blind observers. *Perception & Psychophysics.*, 45: 49-54, 1989.

[HoBS99] Ho C-H., Basdogan C., Srinivasan M.A.: Efficient point-based rendering techniques for haptic display of virtual objects. *Presence: Teleoperators & Virtual Environments.*, 8(5): 477–491, 1999

[HFRY93] Hollins M., Faldowski R., Rao S., Young F.: Perceptual dimensions of tactile surface texture: A multidimensional scaling analysis. *Perception & Psychophysics.*, 54: 679-705, 1993

[HBKY00] Hollins M., Bensmaia S., Karlof K., Young F.: Individual differences in perceptual space for tactile textures: Evidence from multidimensional scaling. *Perception & Psychophysics.*, 62: 1534-1544, 2000

[Howe02] Howe R.: The Haptic Community Web Site- Haptic Research. *Harvard University.*, http://haptic.mech.northwestern.edu/TactileDisplay.html, 2002-04-03

[JPCK*99] Jansson G., Petrie H., Colwell C., Kornbrot D., Fanger J., Konig H., Billberger K., Hardwick A., Furner S.: Haptic Virtual Environments for Blind People: Exploratory Experiments with Two Devices. *Internationl Journal of Virtual Reality* 4: 10-20, 1999

[JoLL82] Johansson E.A., Landstrom U., Lundstrom R.: Responses of mechanoreceptive afferent units in the glabrous skin of the human hand to sinusoidal skin displacements. *Brain Research.*, 244: 17-25, 1982

[Katz89] D. Katz.: The World of Touch. Erlbaum, Hillsdale, NJ, L. Krueger, *Trans.*, (Original work published 1925), 1989

[KKSD02] Kim L., Kyrikou A., Sukhatme G.S., Desbrun M.: An Implicit-based Haptic Rendering Technique. *Proceedings of the IEEE/RSJ International Conference on Intelligent Robots.*, 2002

[KlLe99] Klatzky R.L., Lederman S.J.: Tactile roughness perception with a rigid link interposed between skin and surface. *Perception & Psychophysics.*, 61: 591-607, 1999

[Kuch08] Kuchenbecker K. J: Haptography: capturing the feel of real objects to enable authentic haptic rendering. *Proceedings of the 2008 Ambi-Sys workshop on Haptic user interfaces in ambient media systems*, Quebec City, Canada, Feb. 11-14, 2008

[KyLe09] Kyung K., Lee J.: Ubi-Pen: A haptic interface with texture and vibrotactile display. *IEEE computer graphics and applications.*, 29(1): 56-64, 2009

[LaAn09] Lang J, Andrews S.: Measurement based Modeling of Contact Forces and Textures for Haptic Rendering. *Proceedings of IEEE Transactions on Visualization And Computer Graphics.*,Vol. 2009

[LaDa07] Laycock, S.D., Day A.M.: A survey of haptic rendering techniques. *Computer Graphics Forum.*, vol. 26, no. 1, pp. 50-65, March 2007.

[LeKl87a] Lederman S.J., Klatzky R.L.: Hand Movements: A window into haptic object recognition. *cog Psych.*, 19: 342-368, 1987

[LeKl98b] Lederman S.J., Klatzky R.L.: Feeling through a Probe. *Proceedings of the ASME.,* DWC-Vol.64, 1998

[LKHG00] Lederman S.J., Klatzky R.L., Hamilton C., Grindley M.: Perceiving surface roughness through a probe: Effects of applied force and probe diameter. *Proceedings of the ASME DSCD-IMECE.*, 2000

[LKHG*03] Lederman S.J., Klatzky R.L., Hamilton C, Grindley M, Swendsen RH.: Feeling textures through a probe: Effects of probe and surface geometry and exploratory factors. *Perception & Psychophysics* 65(4): 613-631, 2003

[MaHa04] Mahvash M., Hayward V.: High Fidelity Haptic Synthesis of Contact with Deformable bodies. *IEEE Computer Graphics and Applications.,* 24(2): 48-55, 2004

[MRFV*96] Mark W., Randolph S., Finch M., Verth J.V., Taylor R.M. II.: Adding Force Feedback to Graphics Systems: Issues and Solutions. *Proceedings of the 23rd Annual Conference on Computer Graphics and interactive Techniques SIGGRAPH '96. ACM.,* New York, NY, 447-452, 1996

[MaSa94] Massie T.H., Salisbury J.K.: The Phantom Haptic Interface: A Device for Probing Virtual Objects. *ASME Haptic Interfaces for Virtual Environment and Teleoperator System.*, 1994

[MOSB*90] Minsky M., Ouh-Young M., Steele O., Jr., Brooks F.P., Behensky M.: Feeling and seeing: Issues in force display. *In Rich Riesenfeld and Carlo Sequin, eds., Computer Graphics (1990 Symp. on Interactive 3D Graphics.,)* 24: 235-243, 1990

[Mins95] Minsky M.: Computational Haptics: The Sandpaper System for Synthesizing Texture for a Force-Feedback Display. Ph.D. thesis, Ph.D. Dissertation, *Program in Media Arts and Sciences, MIT, Cambridge*, MA1995. Thesis work done at UNC-CH Computer Science, 1995

[MiLe96] Minsky M., Lederman S.J.: Simulated Haptic Textures: Roughness. Proceedings of ASME Intl. Mech. Eng. Congress.: Dynamic Systems and Control Division (Haptic Interfaces for Virtual Environments and Teleoperator Systems)., 58: 421-426, 1996

[Morg95] Morgenbesser H.B.: Force Shading for Haptic Shape Perception in Haptic Virtual Environments. M.Eng. thesis, MIT, 1995

[OkDH98] Okamura A.M., Dennerlein J.T., Howe R.D.: Vibration feedback models for virtual environments. *Proceedings of the IEEE Int. Conf. on Robotics and Automation* 1: 674-679, 1998

[OkCD01] Okamura A.M., Cutkosky M.R., Dennerlein J.T.: Reality-based model for vibration feedback in virtual environments. *Proceedings of the ASME Dynamic Systems and Control Division.,* pp1117-1124, 2001

[Okam04] Okamura A.M.: Methods for Haptic Feedback in Teleoperated Robot-Assisted Surgery. *Industrial Robot.*, 31(6), pp. 499-508, 2004

[OaLi04] Otaduy M.A., Lin M.C.: A perceptually-inspired force model for haptic texture rendering. *Proceedings of the 1st Symposium on Applied perception in graphics and visualization.*, Los Angeles, California, 2004

[OJSL04] Otaduy M.A., Jain N, Sud A, Lin M.C.: Haptic display of interaction between textured models. *Proceedings of IEEE Visualization.*, pp. 297-304, 2004

[Oxfo09] "Oxford English Dictionary", Oxford University Press 2009, December 2, 2009 <http://www.oed.com/>

[PLLW99] Pai D.K., Lang J., Lloyd J.E., Woodham R.J.: ACME, A telerobotic active measurement facility. *In 6th International Symposium on Experimental Robotics.*, pp. 391-400,1999

[PLLR00] Pai D.K., Lang J., Lloyd J.E., Richmond J.L.: Reality-based Modeling with ACME: A Progress Report. *Proceedings of the International Symposium. on Experimental Robotics.*, 2000

[PaRi03] Pai D., Rizun P.: The WHaT: A Wireless Haptic Texture Sensor. Proceedings of 11th Symposium on Haptic Interfaces for Virtual Environment and Teleoperator Systems., Los Angeles, USA, 2003

[Pala97] Palacherla A.: Implementing IIR Digital Filters. *Microchip Technology Inc.*, 1997

[PaBu87] Parks T.W., Burrus C.S.: Digital Filter Design, *John Wiley & Sons.*, pp.226-28, 1987

[PaHa03] Pasquero J., Hayward V.: STReSS: A Practical Tactile Display System with One Millimeter Spatial Resolution and 700 Hz Refresh Rate. *Proceedings from. Eurohaptics.*, 2003

[PDJL*01] Pai D.K., Doel K., James D.L., Lang J, Lloyd J.E., Richmond J.L., Yau S.H.: Scanning physical interaction behavior of 3D objects. *Proceedings of ACM SIGGRAPH in Computer Graphics (ACM SIGGRAPH 2001)*, pp. 87–96, Aug 2001

[Pasq03] Pasquero J.: STReSS: A Tactile Display using Lateral Skin Stretch. M. Eng Thesis, McGill University. 2003

[Phon75] Phong B.T.: Illumination for Computer Generated Pictures. *Communications of the ACM.*, 18(6): 311-317, 1975

[PDVG03] Picard D., Dacremont C., Valintin D., Giboreau A.: Perceptual dimensions of tactile textures. *Acta Psychologica.,* 114: 165- 184, 2003

[Robl08] Robles-De-La-Torre G.: Principles of Haptic Perception in Virtual Environments. *In Grunwald M (Ed.), "Human Haptic Perception".*, pp. 363-379. Birkhauser Verlag, 2008

[RuKK97]Ruspini D.C., Kolarov K., Khatib O.: The haptic display of complex graphical environment. *Proceedings of SIGGRAPH 97 conference.,* 1:295-301, 1997

[SAGM*05] Shirley P., Ashikhmin M., Gleicher M., Marschner S.R., Reinhard E., Sung K., Thompson W.B., Willemsen P.: Fundamentals of Computer Graphics, 2005

[POINT GREY] http://www.ptgrey.com

[SiPa96] Siira J., Pai D.: Haptic texturing: A stochastic approach. *In International Conference on Robotics and Automation.,* 557—562, 1996

[TiKa06] Tiest W.M.B., Kappers A.M.L.: Analysis of haptic perception of materials by multidimensional scaling and physical measurements of roughness and compressibility. *Acta Psychology.,* 121: 1-20, 2006

[Verl67] Verlet L.: Computer experiments on classical fluids. *Phys. Rev.*, vol. 159, no. 1, pp. 98, July 1967.

[Wagn09] Wagner D.: Handheld Augmented Reality. *Graz University of Technology.,* http://studierstube.icg.tu-graz.ac.at/handheld_ar/artoolkitplus.php, 2009-09-06

[WaWa92] Watt A., Watt M.: Advanced Animation and Rendering Techniques: *Theory and Practice*, Addison-Wesley, 1992

[WeHo95] Wellman P., Howe R.D.: Towards realistic vibrotactile display in virtual environments. *American Society of Mechanical Engineers, Dynamic Systems and Control Division.*, 57(2):713-718, 1995

[ZiSa94] Zilles C., Salisbury J.K .: A Constraint-based God-object Method For Haptic Display. *ASME Haptic Interfaces for Virtual Environment and Teleoperator System.*, 1994